Electronic Supplementary Material (ESI) for Journal of Materials Chemistry C.

Electronic supplementary information

A bis(diketopyrrolopyrrole) dimer-containing ligand in platinum(II) polyyne oligomer exhibiting ultrafast photoinduced electron transfer with PCBM and solar cell properties

Mélodie Nos, †[a] Gabriel Marineau-Plante, †[b] Di Gao,[a] Muriel Durandetti,[c] Julie Hardouin,[d,e] Paul-Ludovic Karsenti, [b] Gaurav Gupta,[f] Ganesh D. Sharma,*[f] Pierre D. Harvey,* [b] Cyprien Lemouchi,*[a] Loïc Le Pluart*[a]

a NORMANDIE UNIV, ENSICAEN, UNICAEN, CNRS, LCMT, 14000 CAEN, FRANCE

b Département de chimie, Université de Sherbrooke, Sherbrooke, PQ, Canada J1K 2R1

c Normandie Univ, UNIROUEN , INSA Rouen, CNRS, COBRA, 76000 Rouen, France

d Normandie Univ, UNIROUEN , INSA Rouen, CNRS, PBS, 76000 Rouen, France

e PISSARO Proteomic Facility, IRIB, F-76820 Mont-Saint-Aignan, France

f Department of Physics, LNM Institute of Information Technology (Deemed to be University), Jamdoli 302017 Jaipur, India

Email:
[a]cyprien.lemouchi@ensicaen.fr, loic.le_pluart@ensicaen.fr
[b] Pierre.Harvey@USherbrooke.ca

Contents

1.Ligands synthesis and characterization

Synthetic route to the diethynyl ligand **L1**

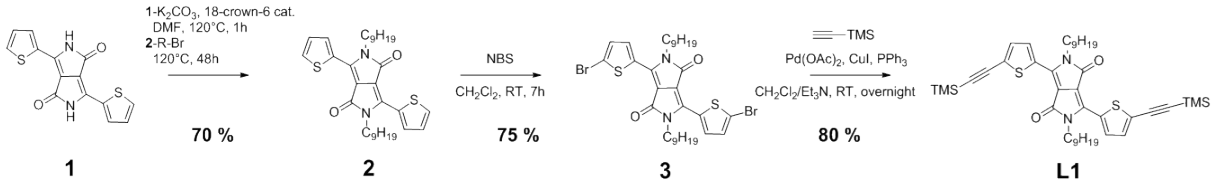

Scheme S1 : synthetic route for the **L1** preparation

1

3,6-Bis(thiophen-2-yl)-2H,5H-pyrrolo[3,4-*c*]pyrrole-1,4-dione

The procedure was inspired from the literature, C. H. Woo, P. M. Beaujuge, T. W. Holcombe, O. P. Lee, J. M. J. Fréchet, J. Am. Chem. Soc. ***2010****, 132, 15547*. In a flame-dried 250 ml bicol, sodium metal (Na (0)) (2.4 g, 104.39 mmol) was slowly added to the 2-methylbutan-2-ol (100 mL) at 120°C. The mixture was stirred at 120 °C until complete dissolution of Na(metal). The temperature was decreased to 90 °C and the 2-thiophenecarbonitrile (8.52 g, 78.06 mmol) was added in one portion, affording a brown coloration of the reaction mixture. Afterwards, a solution of diethyl succinate (6.18 g, 35.48 mmol) was added dropwise and the mixture was stirred at 120 °C overnight. The solution turned progressively to dark purple. After cooling to room temperature, the mixture was poured into dilute HCl (1N, 100 mL) and was stirred vigorously for 1h at 0°C. The precipitated deep purple solid **1** was collected by filtration under vacuum. The solid was washed several times with methanol and dried under vacuum to give a purple powder (5.75 g, 19.14 mmol, 54 % yield) and used without further purification.^{1}H NMR (400 MHz, DMSO) δ (ppm): 11.24 (s, 1H), 8.23 (s br., 1H), 7.96 (br., 1H), 7.30 (s br., 1H). ^{13}C NMR (400 MHz, DMSO) δ (ppm): 161.61, 136.14, 132.63, 131.25, 130.78, 128.69, 108.54.

2

2,5-Dinonyl-3,6-bis(thiophen-2-yl)pyrrolo[3,4-*c*]pyrrole-1,4-dione

The procedure was inspired from the literature, S. Jung Park , J. E. Jung , M. K. Kang , Y. H. Na, H. H. Song , J. W. Kang , N. S. Baek , T.-D. Kim , Synthetic Metals, ***2015****, 203, 221.* In a 250 mL flame-dried Schlenk, **1** (1.4 g, 4.67 mmol), anhydrous potassium carbonate (2.58 g, 18.67 mmol) and 18-crown-6 (cat., 5 mg) were added in freshly distilled DMF (70 mL). The mixture was stirred at 100 °C for 1 h under argon atmosphere. 1-bromononane (2.89 g, 13.95 mmol)

was added dropwise and the reaction mixture was stirred at 100 °C for 36 h, monitored in TLC (R_f = 0.6, using $CHCl_3$ as eluent). When the reaction was complete, the reaction mixture was cooled to room temperature and extracted with CH_2Cl_2 (200 mL). The isolated organic layer was washed with brine (4 x 100 mL), dried over $MgSO_4$, filtered and evaporated under reduced pressure. The crude material was purified by chromatography using silica gel with $CHCl_3$ as eluent to afford **2** as a purple solid (1.80 g, 3.26 mmol, 70 % yield). ^{1}H NMR (500 MHz, $CDCl_3$) δ (ppm): 8.86 (dd, 2H, *J* = 4.0 Hz, *J* = 1.0 Hz), 7.57 (dd, 2H, *J* = 5.0 Hz, *J* = 1.1 Hz), 7.21 (t, 2H, *J* = 4.5 Hz), 4.0 (t, 4H, *J* = 8.0 Hz), 1.74-1.68 (m, 4H), 1.41-1.36 (m, 4H), 1.34-1.29 (m, 4H), 1.27-1.23 (m, 19H), 0.84 (m, 6H). ^{13}C NMR (500 MHz, $CDCl_3$) δ (ppm): 161.59, 140.42, 135.50, 130.90, 130.02, 128.84, 107.91, 42.48, 32.10, 30.22, 29.96, 29.74, 29.49, 27.13, 22.92, 14.37. IR (cm^{-1}): v = 3069 (v, C-H aromatic), 2918 and 2848 (w, v (C-H)), 2145, 1655 (w, v(C=O)). MS-ASAP-TOF *(m/z)*: calc. for $C_{32}H_{44}N_2O_2S_2$ (**2**) $[M+H]^+$, m/z = 553.28 ; measured $[M+H]^+$ m/z = 553.29. $T_{m.p}$ (°C) = 154.

3

3,6-bis-(5-bromothiophen-2-yl)-2,5-dinonyl-2,5-dihydropyrrolo[3,4-c]pyrrole-1,4-dione

The procedure was inspired from the literature, C. Wang, Y. Qin, Y. Sun, Y-S. Guan, W. Xu, D. Zhu, *ACS Appl. Mater. Interfaces,* **2015**, *7*, 15978. In a 100 mL round bottom flask wrapped with an aluminum foil, **2** (735.0 mg, 1.33 mmol) was dissolved in CH_2Cl_2 (50 mL) and *N*-bromosuccinimide (521.0 mg, 2.93 mmol) and was added in a single portion. The mixture was stirred at room temperature for 7 hrs and monitored by TLC (R_f=0.5 using CH_2Cl_2/pentane: 70/30). The product was precipitated after addition of methanol (50 mL) to the concentrated reaction mixture. The dark purple solid **3** (708.22 mg, 1.00 mmol, 75% yield) was isolated after filtration, washed with cold methanol (2 × 200 mL) and dried under vacuum. ^{1}H NMR (400 MHz, $CDCl_3$) δ (ppm) : 8.63 (d, 2H, *J* = 4.3 Hz), 7.23 (d, 2H, *J* = 4.3 Hz), 3.93 (t, 4H, *J* = 7.9 Hz), 1.69 (m, 4H), 1.41-1. 36 (m, 4H), 1.34-1.31 (m, 5 H), 1.28-1.24 (m, 20 H), 0.86 (m, 7H). ^{13}C NMR (500 MHz, $CDCl_3$) δ (ppm): 161.06, 139.00, 135.24, 131.62, 131.19, 119.05, 107.95, 31.81, 29.95, 29.40, 29.16, 26.80, 22.61, 14.01. IR (cm^{-1}): v = 3092 (v, C-H aromatic), 2916 and 2.851 (w, v (C-H)), 1660 (w, v(C=O)) and 1558. MALDI-TOF (dithranol) calc. for $C_{32}H_{42}Br_2N_2O_2S_2$ (**3**) $[M^{\bullet+}]$, m/z = 708.11; measured $[M^{\bullet+}]$ m/z = 708.10 ; $T_{m.p}$ (°C) =175.

Synthetic route to the diethynyl ligand **L4**

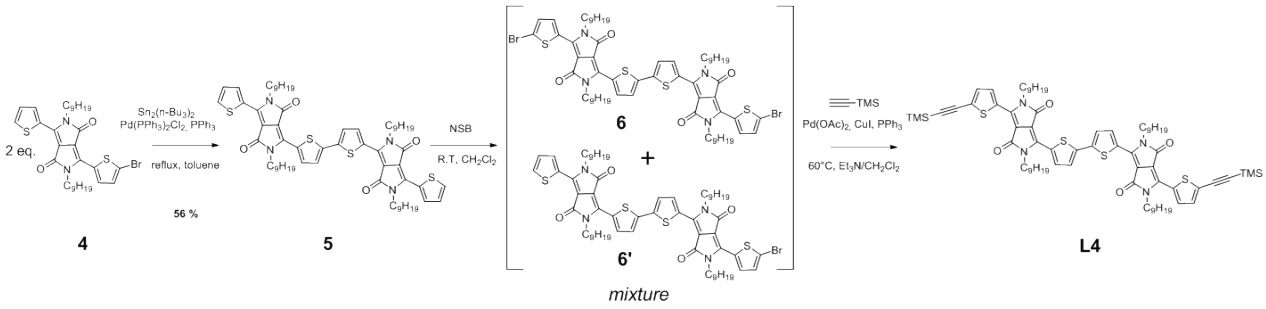

Scheme S2: synthetic route for the **L4** preparation

4

3-(5-bromothiophen-2-yl)-2,5-dinonyl-6-(thiophen-2-yl)-2,5-dihydropyrrolo[3,4-c]pyrrole-1,4-dione

The procedure was inspired from the literature, P.-Y. Ho, B. Zheng, D. Mark, W.-Y. Wong, D. W. McCamant, R. Eisenberg, Inorg. Chem. ***2016****, 55, 8348.* In a 250 mL round bottom flask wrapped with an aluminum foil, **2** (871.0 mg, 1.58 mmol) was dissolved in CH_2Cl_2 (50 mL). *N*-bromosuccinimide (281.20 mg, 1.58 mmol) was added in a single portion. The mixture was stirred at room temperature for 6.5 hrs. The product was precipitated upon addition of methanol to the concentrated reaction mixture. The dark purple solid **4** (697.88 mg, 1.10 mmol, 70% yield) was isolated after filtration, washed with cold methanol (2 × 200 mL) and dried under vacuum. ^{1}H NMR (500 MHz, $CDCl_3$) δ (ppm): 8.91 (d, 1H, *J* = 4.0 Hz), 8.64 (d, 1H, *J* = 4.2 Hz), 7.63 (d, 1H, *J* = 4.7 Hz), 7.26 (t, 1H, *J* = 4.5 Hz), 7.20 (d, 1H, *J* = 4.3 Hz), 4.03 (t, 2H, *J* = 7.8 Hz), 3.96 (t, 2H, *J* = 7.7 Hz), 1.74-1.65 (m, 4H), 1.41-1. 34 (m, 4H), 1.33-1.23 (m, 23H), 0.84 (m, 6H). ^{13}C NMR (500 MHz, $CDCl_3$) δ (ppm): 161.30, 161.14, 140.48, 138.47, 135.51, 135.08, 131.65, 131.57, 131.23, 130.96, 129.73, 128.69, 118.77, 107.97, 101.61, 42.29, 42.27, 31.85, 30.01, 29.96, 29.48, 29.45, 29.23, 26.88, 26.84, 22.67, 14.11. IR (cm^{-1}): v = 3091 (v, C-H aromatic), 2918 and 2851 (w, v (C-H)), 1658 (w, v(C=O)). MS-ASAP-TOF (m/z) calc. for $C_{32}H_{43}BrN_2O_2S_2$ (**4**), m/z = 630.19 $[M^{\text{Cs}}]^+$, 632.19$[M^{\text{Cs}}+2]^+$, measured m/z = 630.20 and 632.20 ; $T_{m.p}$ (°C) =172.

5

6,6'-([2,2'-bithiophene]-5,5'-diyl)bis(2,5-dinonyl-3-(thiophen-2-yl)-2,5-dihydropyrrolo[3,4-c]pyrrole-1,4-dione)

The procedure was inspired from the literature, A. Riano, P. Mayorga Burrezo, M. J. Mancheno, A. Timalsina, J. Smith, A. Facchetti, T. J. Marks, J. T. Lopez Navarrete, b J. L. Segura, J. Casado, R. Ponce Ortiz, J. Mater. Chem. C, ***2014****, 2, 6376.* In a flame-dried schlenk, the solution of **4** (2.05 g, 3.24 mmol) and hexabutyldistannane (2.69 g, 4.64 mmol) in anhydrous toluene (60 mL) was degassed with an argon stream before adding $Pd(PPh_3)_2Cl_2$ (210.56 mg, 0.30 mmol, 10 mol%) and PPh_3 (157.36 mg, 0.60 mmol, 20 mol %). The mixture was refluxed overnight under argon and monitored by TLC (R_f = 0.40, using CH_2Cl_2/pentane: 40/60). After cooling, the solvent was evaporated under reduced pressure. The resulting solid was extracted from CH_2Cl_2/methanol: 50 mL/100 mL to deliver the product **5** as a dark purple solid (2.0 g, 1.81 mmol, 56 % yield) after a filtration and a washing with methanol. ^{1}H NMR (500 MHz, $CDCl_3$, δ (ppm) : 8.91-8.90 (m, 4H), 7.62 (d, 2H, *J* = 4.8 Hz), 7.43 (d, 2H, *J* = 4.1 Hz), 7.29 (t, 2H, *J* = 4.5 Hz), 4.08 (m, 8 H), 1.78-1.72 (m, 8 H), 1.45-1.40 (m, 8 H), 1.36-1.33 (m, 8H), 1.27-1.24 (m, 38H*), 0.87 (t, 12H*) *: *nonyl side chains on DPP + supplementary hydrogens from aliphatic residue such as pentane*. ^{13}C NMR (500 MHz, $CDCl_3$, δ (ppm): 161.27, 161.25, 140.93, 140.20, 138.73, 136.44, 135.60, 135.27, 130.99, 129.75, 128.62, 126.29, 108.71, 107.94, 42.33, 42.26, 31.86, 30.09, 29.98, 29.51, 29.50, 29.26, 29.23, 26.92, 26.90, 22.67, 14.12. IR (cm^{-1}): v = 3083 (v, C-H aromatic), 2922 and 2850 (w, v (C-H)), 1662 (w, v(C=O)). MALDI-TOF (dithranol) calc. for $C_{64}H_{86}N_4O_4S_4$ (**5**) $[M+H]^+$, m/z = 1103.55 ; measured $[M+H]^+$ m/z = 1103.56 ; $T_{m.p}$ (°C) =228.

6

6,6'-([2,2'-bithiophene]-5,5'-diyl)bis(3-(5-bromothiophen-2-yl)-2,5-dihydropyrrolo[3,4-c]pyrrole-1,4-dione)

The procedure was inspired from the literature, A. Riano, P. Mayorga Burrezo, M. J. Mancheno, A. Timalsina, J. Smith, A. Facchetti, T. J. Marks, J. T. Lopez Navarrete, J. L. Segura, J. Casado, R. Ponce Ortiz, J. Mater. Chem. C, ***2014****, 2, 6376.* In a 50 mL round bottom flask wrapped with an aluminum foil, **5** (208.0 mg, 0.19 mmol) was dissolved in CH_2Cl_2 (30 mL). *N*-bromosuccinimide (84.0 mg, 0.47 mmol, 2.5 eq.) was added in a single portion. The mixture was stirred at room temperature for 9 hrs and was monitored by TLC (R_f = 0.4, using CH_2Cl_2/pentane 40/60). The reaction mixture was evaporated and the resulting solid was extracted in methanol. The solid

was isolated after filtration and washed with cold methanol (2 × 100 mL) and dried under vacuum to give a dark blue solid (173.0 mg). The solid consisted of a mixture between the mono- and the di-brominated product **6'** and **6**. Since the separation of those products was very difficult. The crude material was directly engaged in the next step. MALDI-tof (dithranol) calc. for $C_{64}H_{84}Br_2N_4O_4S_4$ (**6**) m/z = 1258.37 $[M^{\bullet}]^+$, 1260.37$[M^{\bullet}+2]^+$, 1262.37 $[M^{\bullet}+4]^+$ measured m/z = 1258.55, 1260.55 and 1262.55 ; calc. for $C_{64}H_{85}BrN_4O_4S_4$ (**6'**), m/z = 1180.46 $[M^{\bullet+}]$, 1182.46 $[M^{\bullet}+2]^+$; measured m/z = 1180.64 and 1182.64

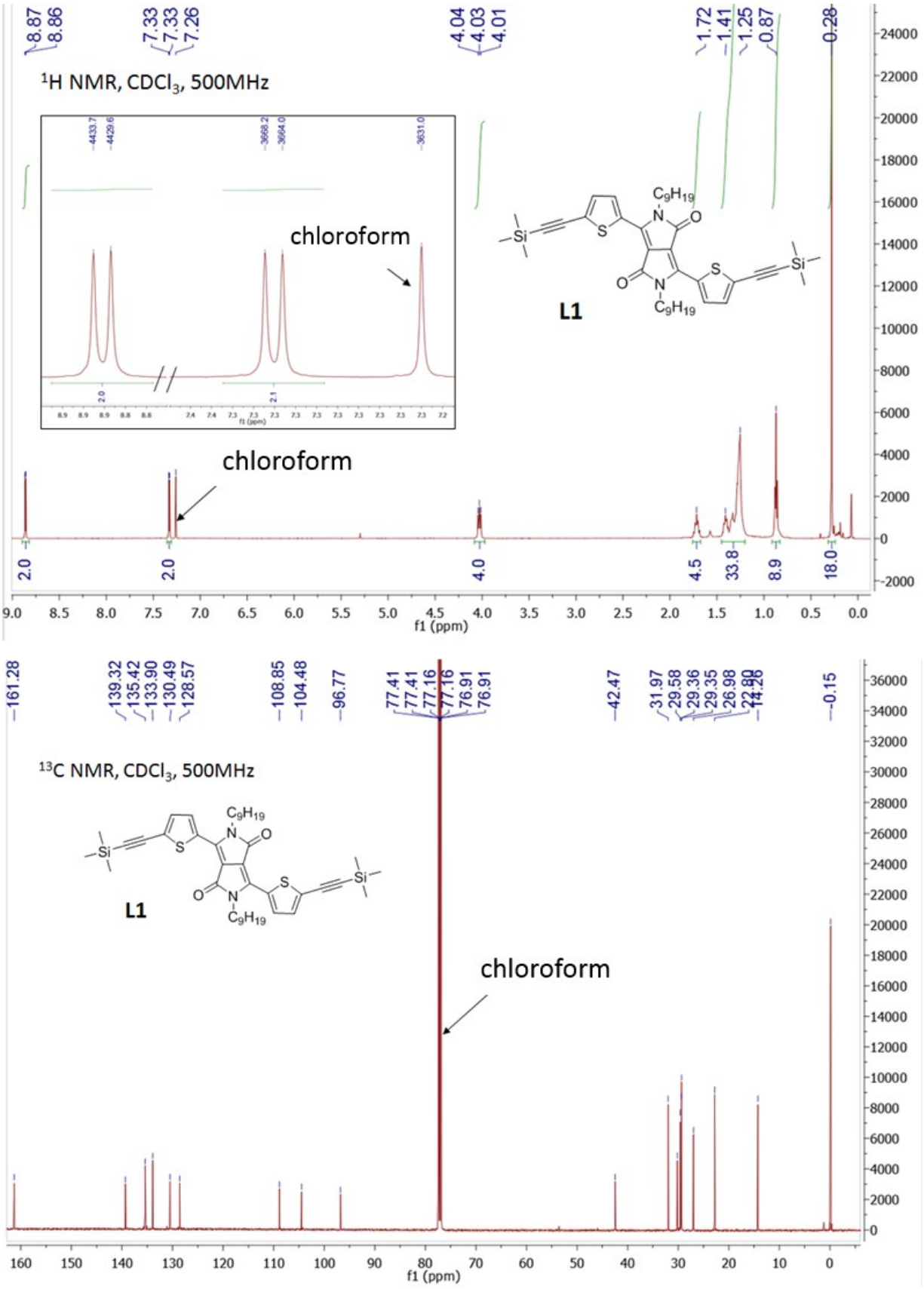

Figure S1: ^{1}H and ^{13}C NMR spectra of **L1** in $CDCl_3$

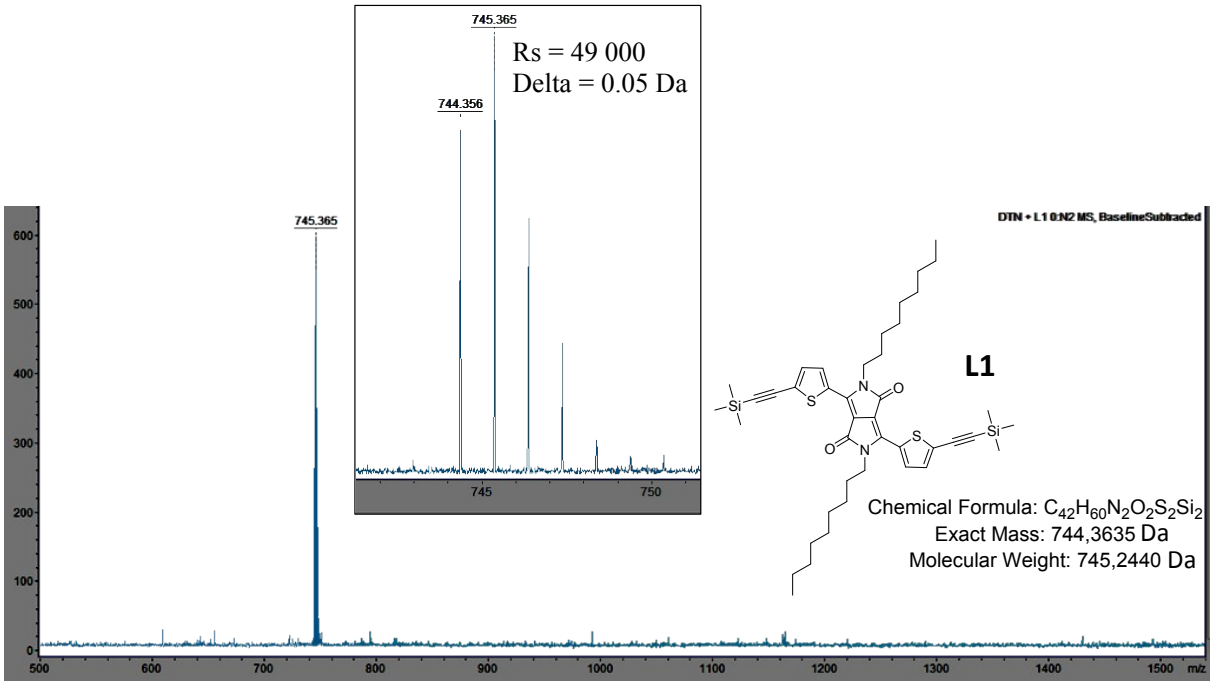

Figure S2: High-resolution ESI-MS (HR-MS) of **L1**

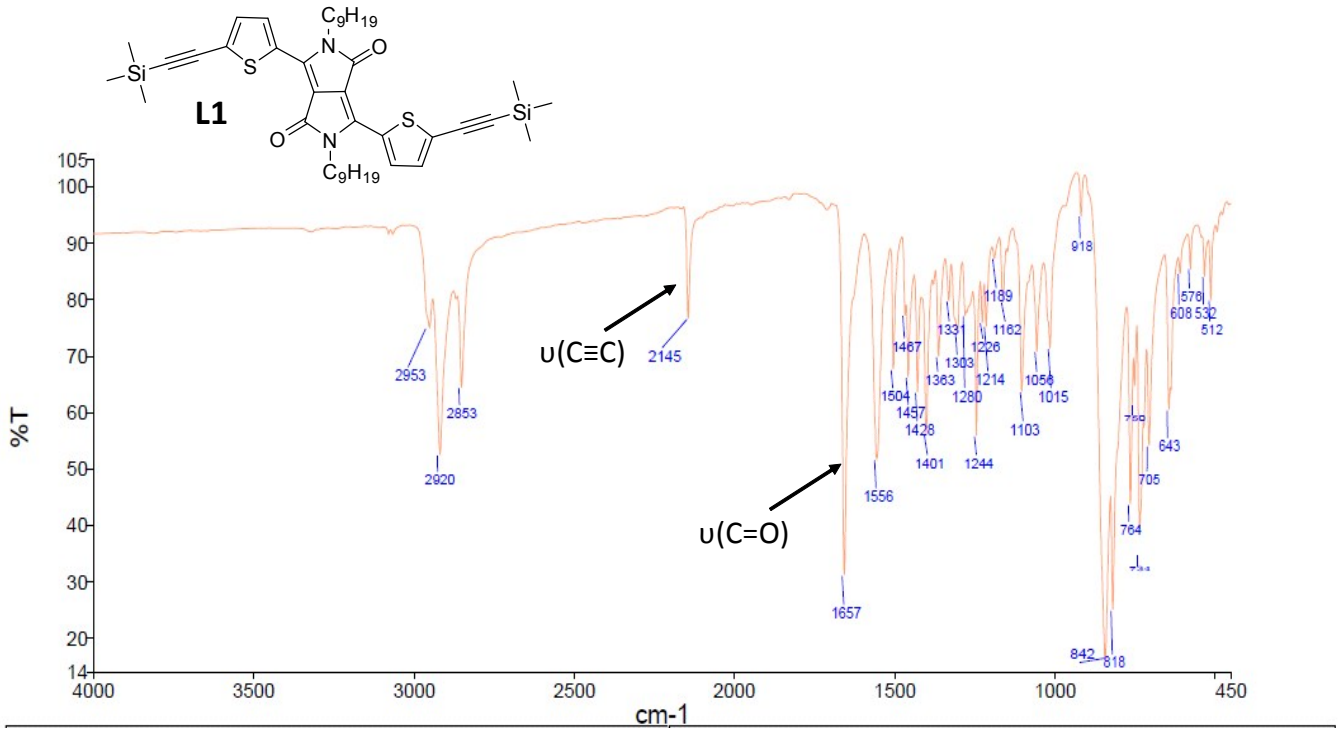

Figure S3: IR ATR spectrum of **L1**

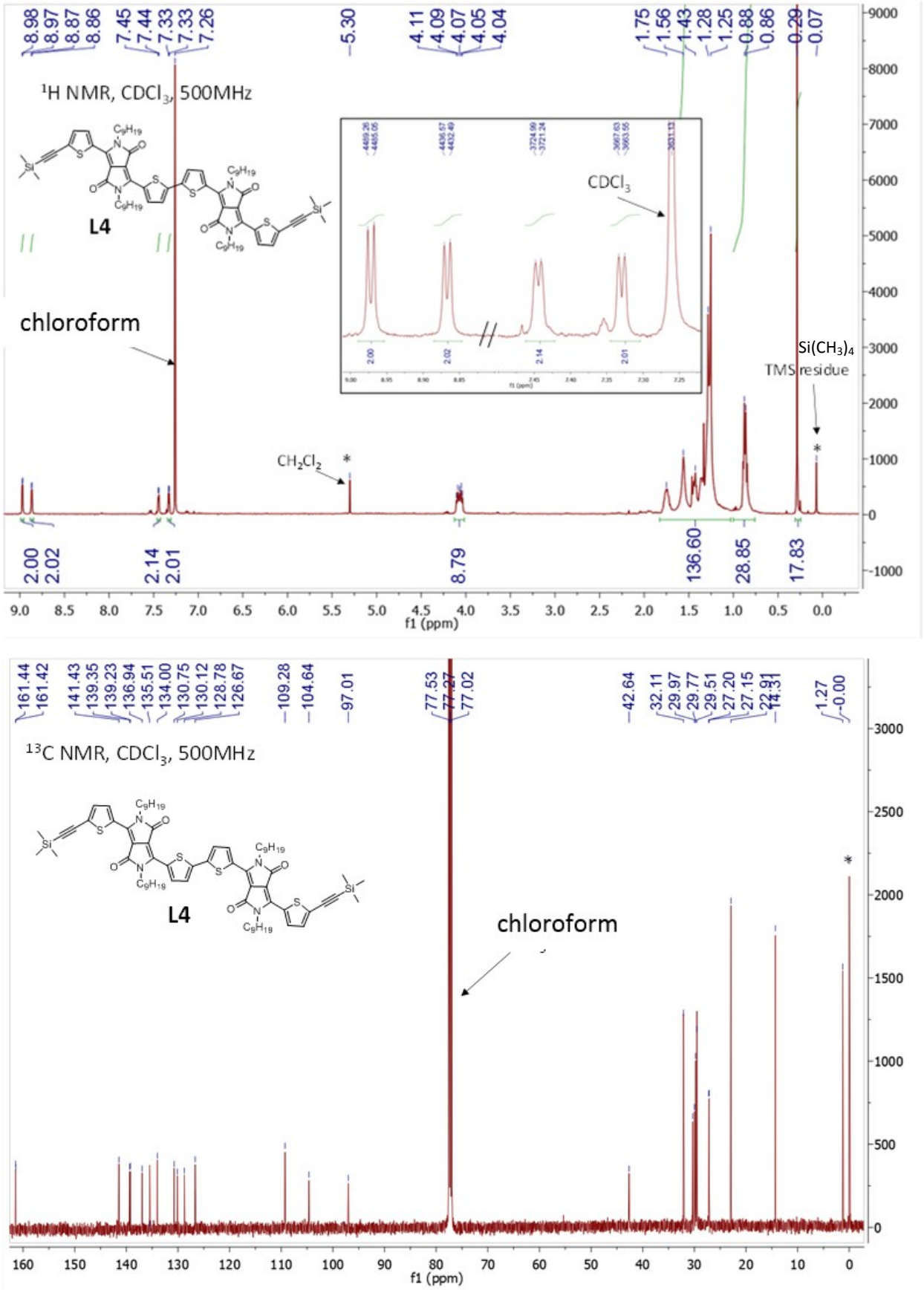

Figure S4: ^{1}H and ^{13}C NMR spectra of **L4** in $CDCl_3$

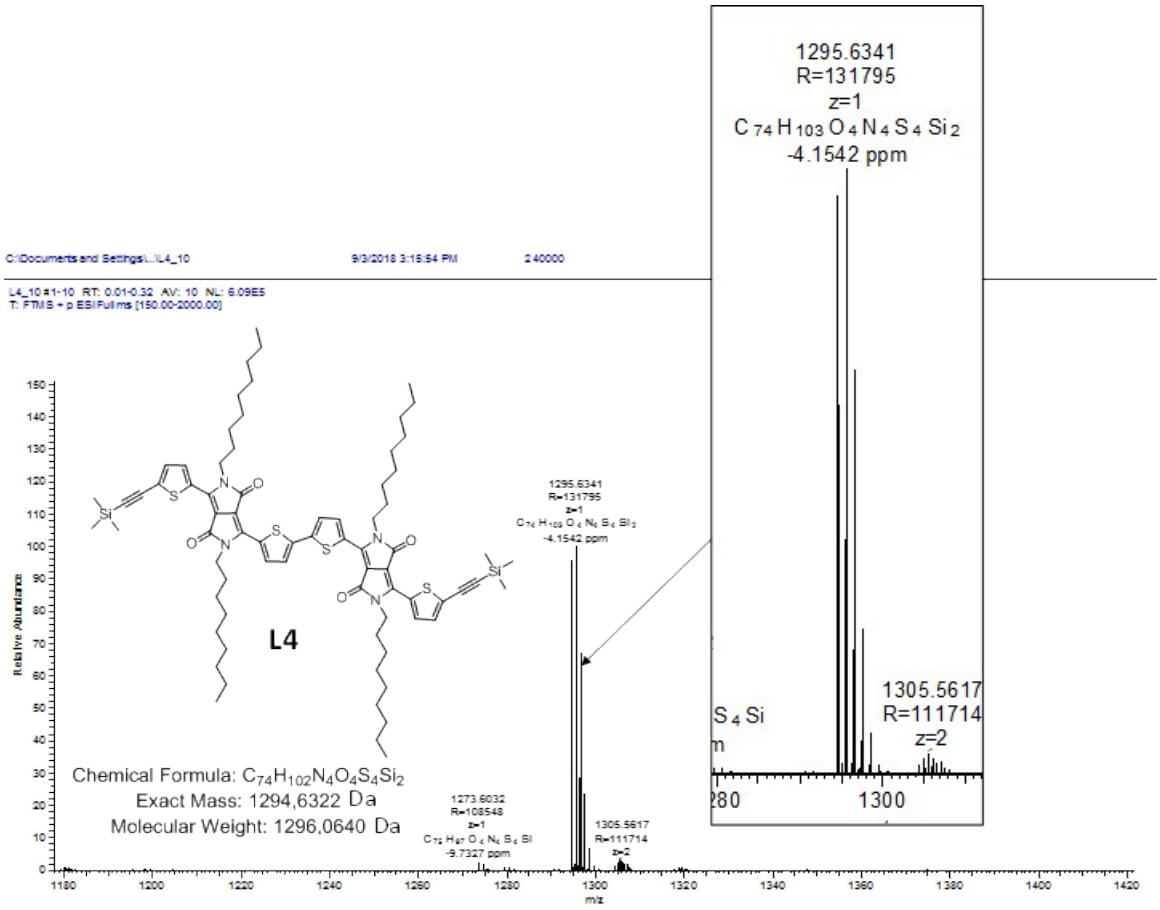

Figure S5: High-resolution ESI-MS (HR-MS) of **L4**

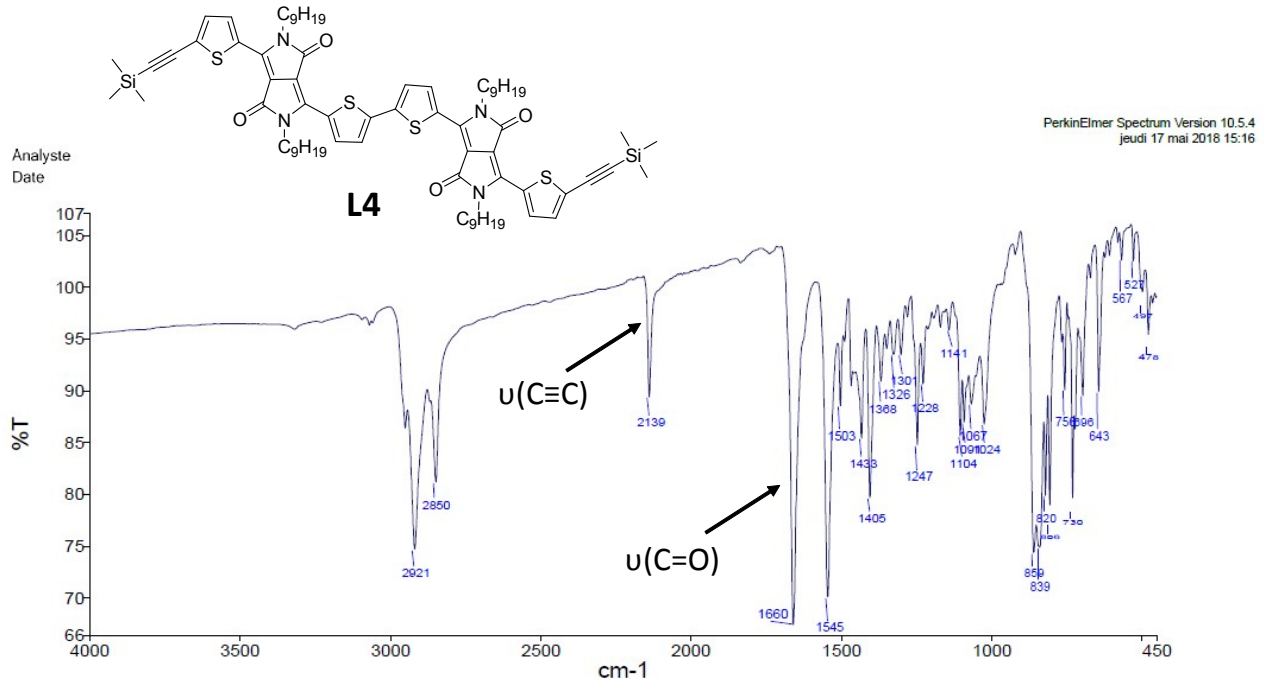

Figure S6: IR ATR spectrum of **L4**

2. Optical Properties of the ligands

Absorption spectra of the ligands **L1** and **L4** in CH_2Cl_2, molar extinction coefficient determination (ε_λ)

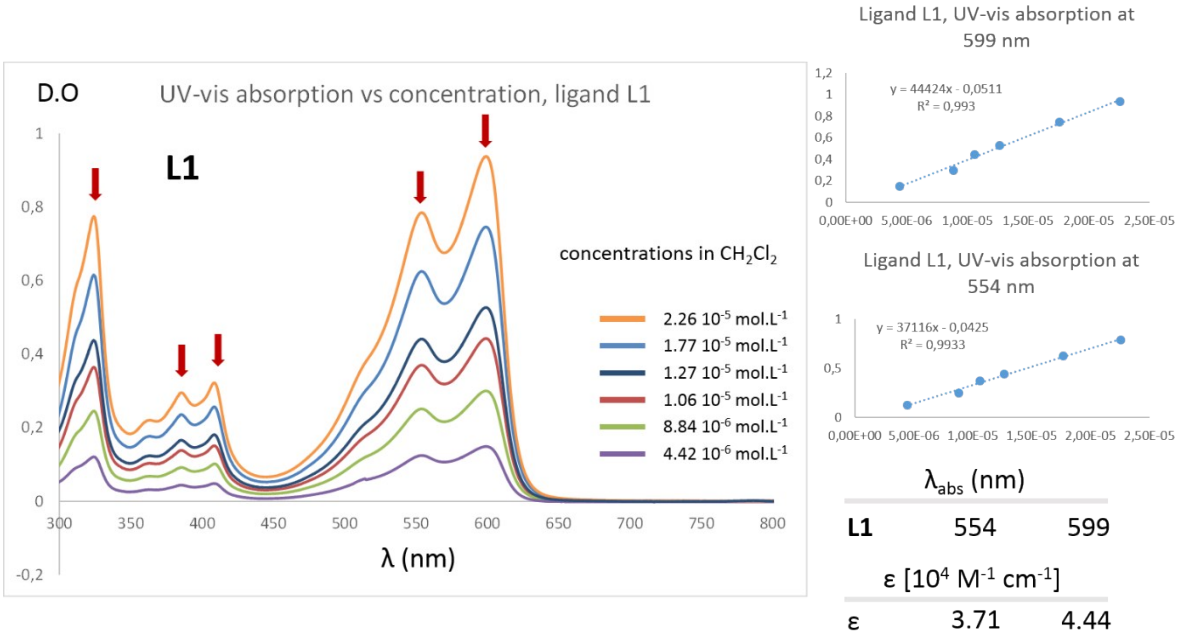

	λ_{abs} (nm)	
L1	554	599
	ε [10^4 M^{-1} cm^{-1}]	
ε	3.71	4.44

Figure S7: Absorption spectra of the ligand **L1** in CH_2Cl_2 at different molar concentrations to calculate the molar extinction coefficient (ε_λ)

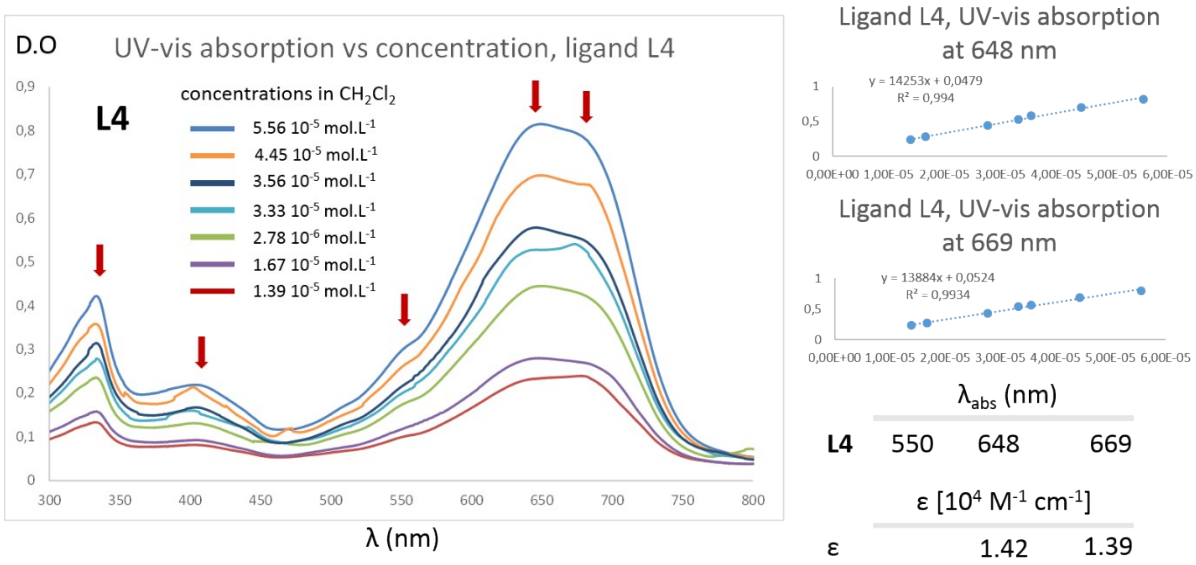

	λ_{abs} (nm)		
L4	550	648	669
	ε [10^4 M^{-1} cm^{-1}]		
ε		1.42	1.39

Figure S8: Absorption spectra of the Ligand **L4** in CH_2Cl_2 at different molar concentrations to calculate the molar extinction coefficient (ε_λ).

3. Metallooligomer characterization

Metallooligomers ^{1}H and ^{31}P NMR spectra

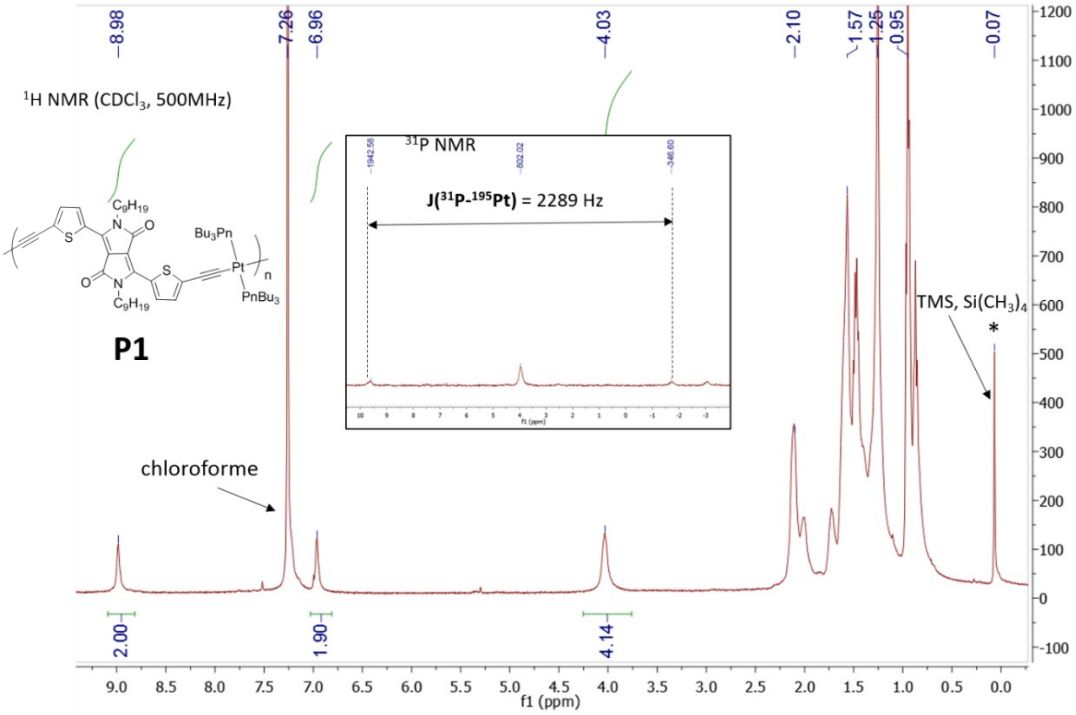

Figure S9: ^{1}H and ^{31}P NMR spectra of the metallooligomers **P1** in $CDCl_3$

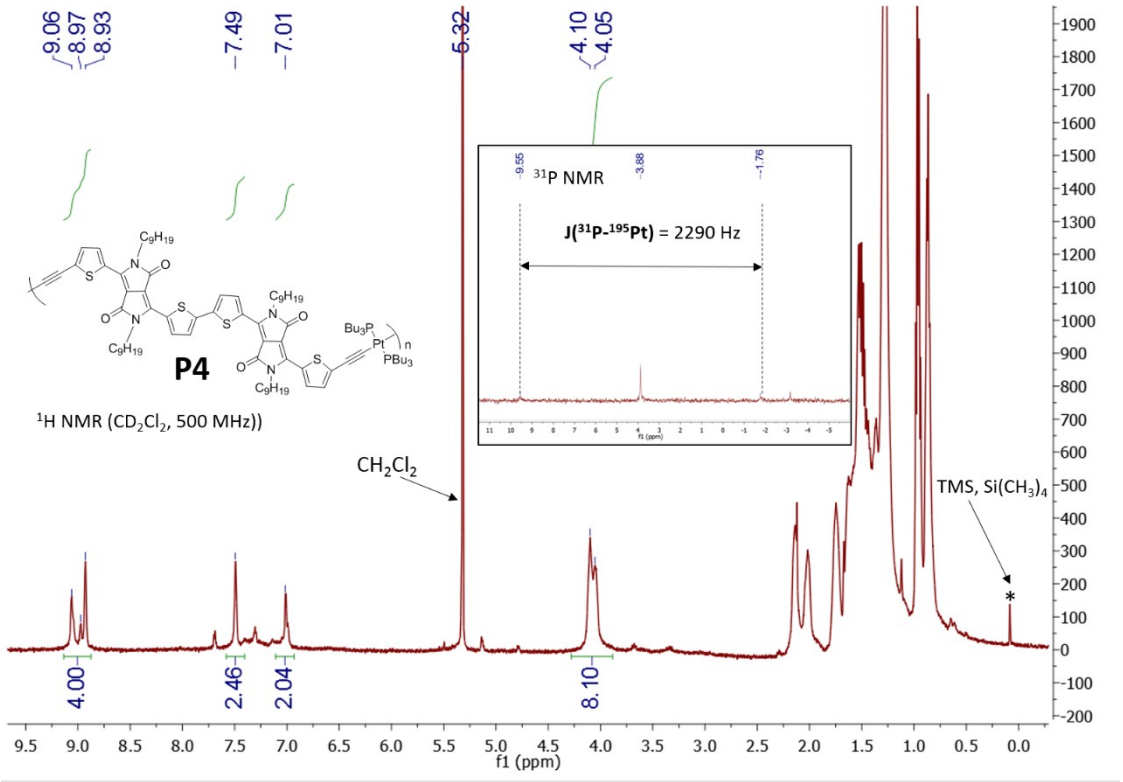

Figure S10: ^{1}H and ^{31}P NMR spectra of the metallooligomers **P4** in CD_2Cl_2

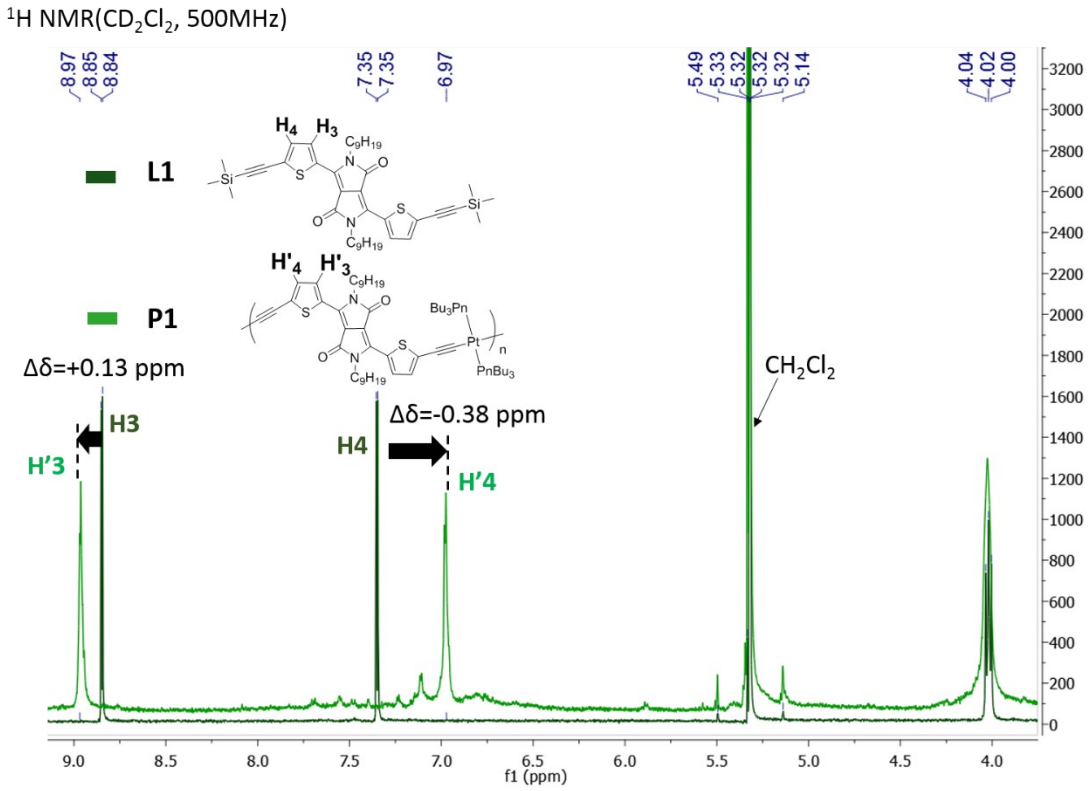

Figure S11: ^{1}H chemical shift's comparison between ligand **L1** and the metallooligomers **P1** in CD_2Cl_2

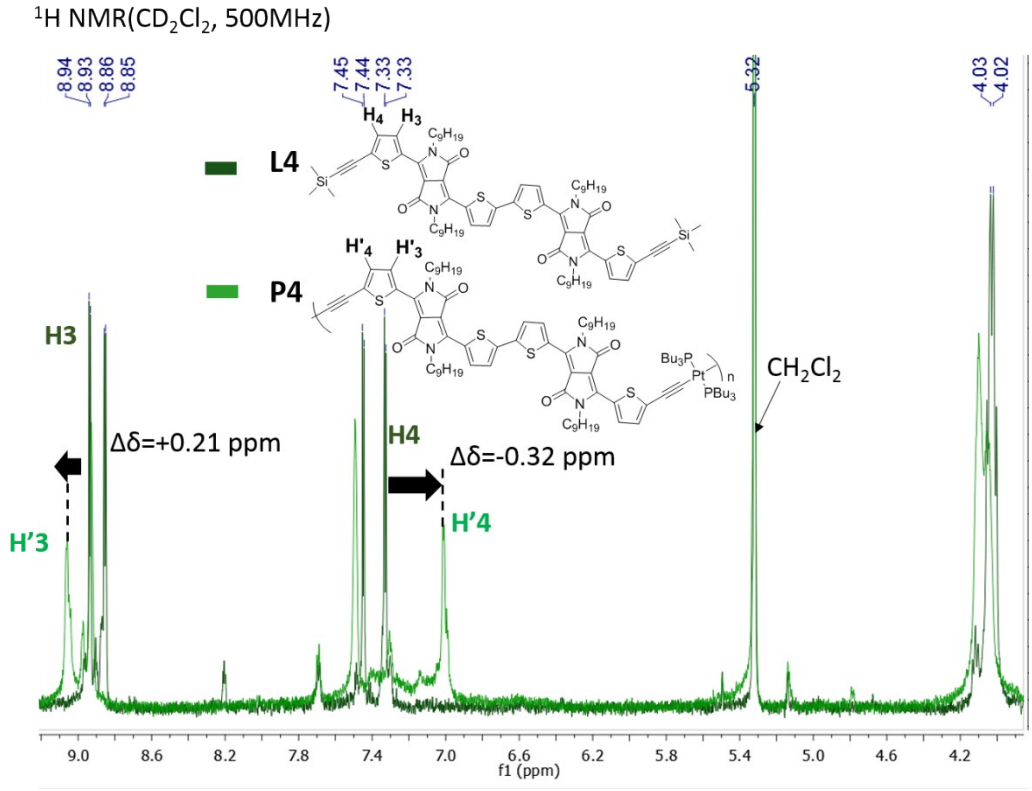

Figure S12: ^{1}H chemical shift comparison between ligand **L4** and metallooligomers **P4** in CD_2Cl_2

IR ATR spectra of the metallooligomers

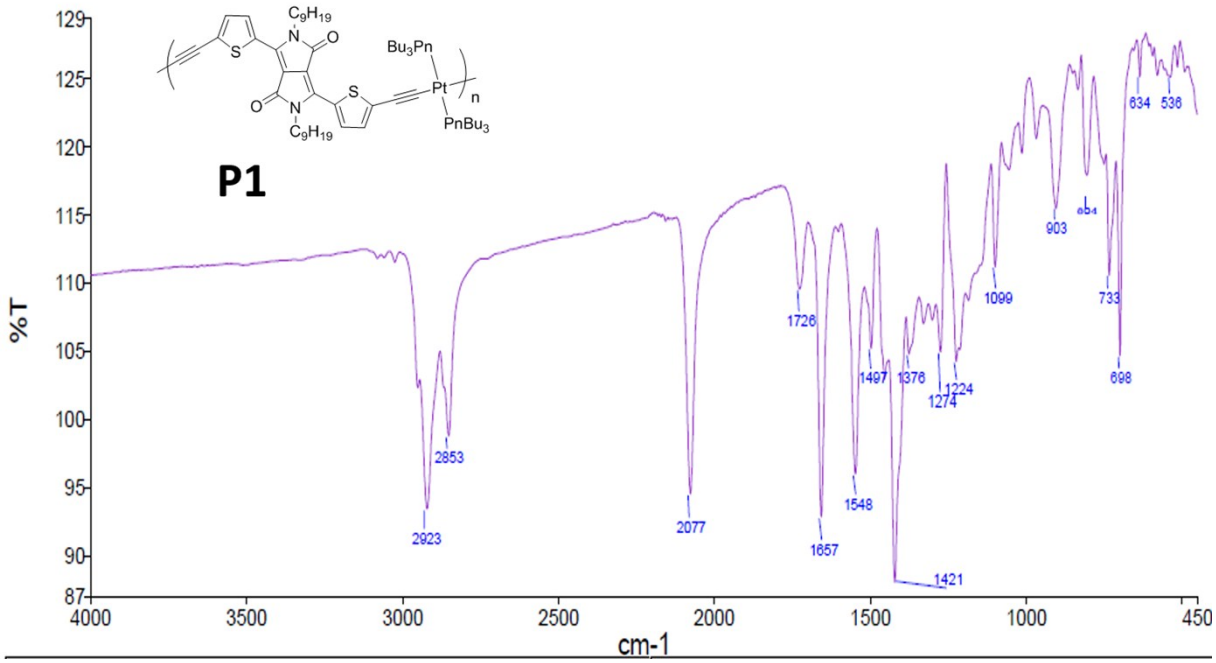

Figure S13: IR ATR spectrum of **P1**

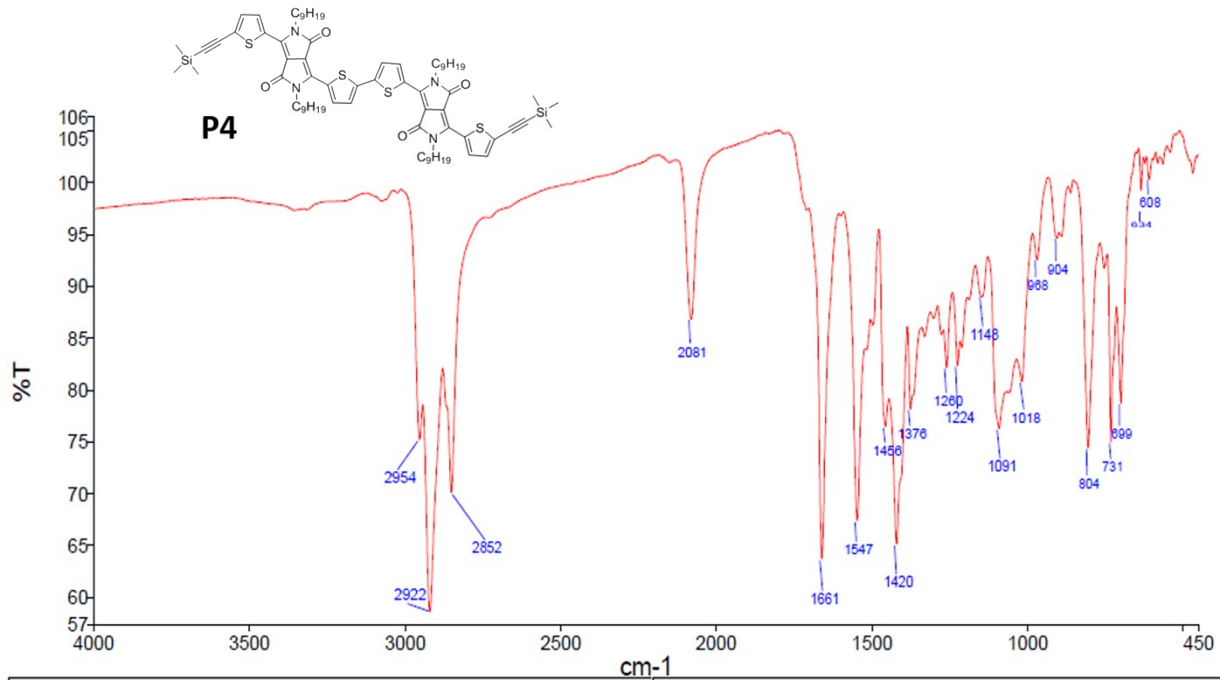

Figure S14: IR ATR spectrum of **P4**

4. GPC analysis

Number- and weight-average molar mass (M_n and M_w respectively) as well as the dispersity (Đ) were determined by gel permeation chromatography (GPC) against polystyrene standards in THF with a flow rate of 1 mL/min

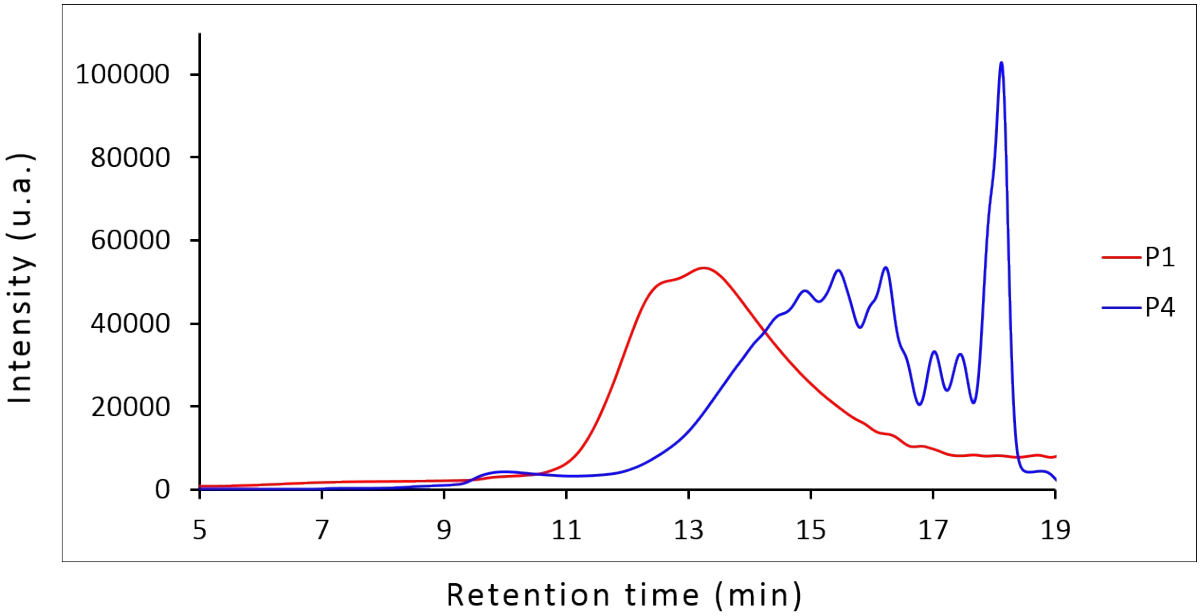

	P1	P4
Mn (g.mol^{-1})	18200	6600
Mw (g.mol^{-1})	38900	73000
$Đ_m$	2.1	11.1
units number	14-15	3-4

Figure S15: GPC chromatograms of the metallooligomers **P1** and **P4**

5. MALDI-TOF of the metallooligomers **P1** and **P4**

The analysis of the metallooligomers **P1** and **P4** by matrix-assisted laser desorption/ionization time-of-flight mass spectrometry (MALDI-TOF/MS) were performed with the 2-[(2E)-3-(4-tert-Butylphenyl)-2-methylprop-2-enylidene]malononitrile (DCTB) matrix, in solution with a concentration of 10 mg mL^{-1} in methylene dichloride following the literature procedure[1].

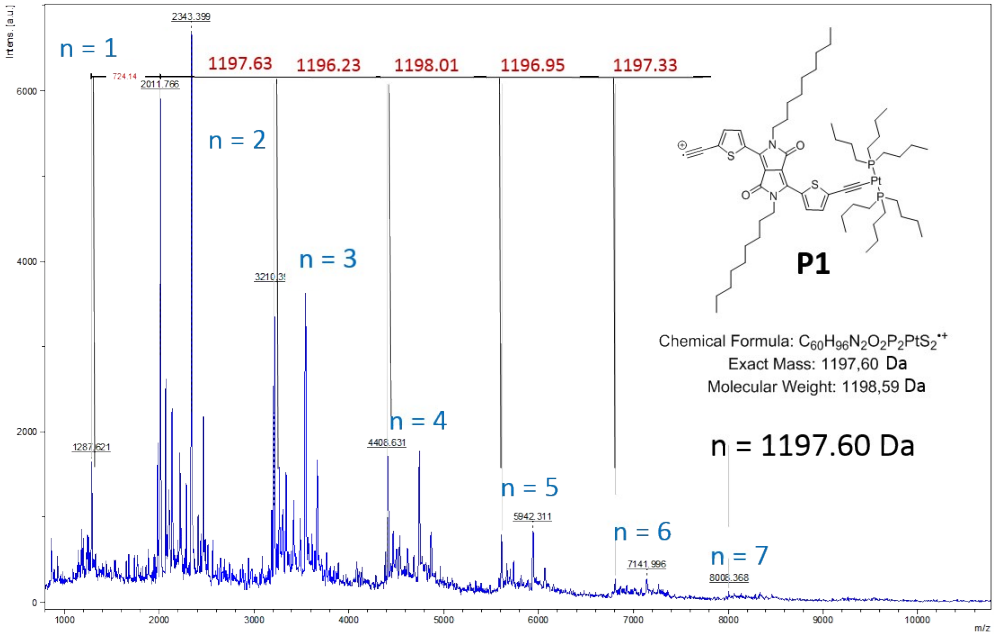

Figure S16: MALDI-TOF spectra of **P1**

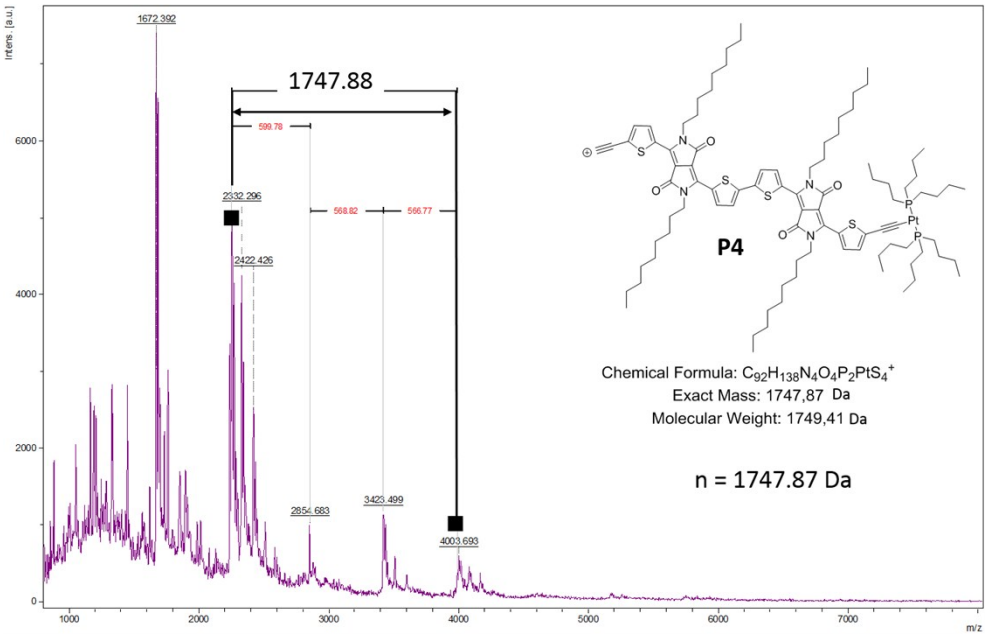

Figure S17: MALDI-TOF spectra of **P4**

[1] (a) M. F. Wyatt,B. K. Stein, A. G. Brenton, *Anal. Chem*. **2006,** 78, 199. (b) J. Mei, K. Ogawa, Y.-G. Kim, N. C. Heston, D. J. Arenas, Z. Nasrollahi, T. D. McCarley, D. B. Tanner, J. R. Reynolds, K. S. Schanze, *Applied Mat Interfaces*, **2009**, 1,150.

6. Thermogravimetric analysis (TGA)

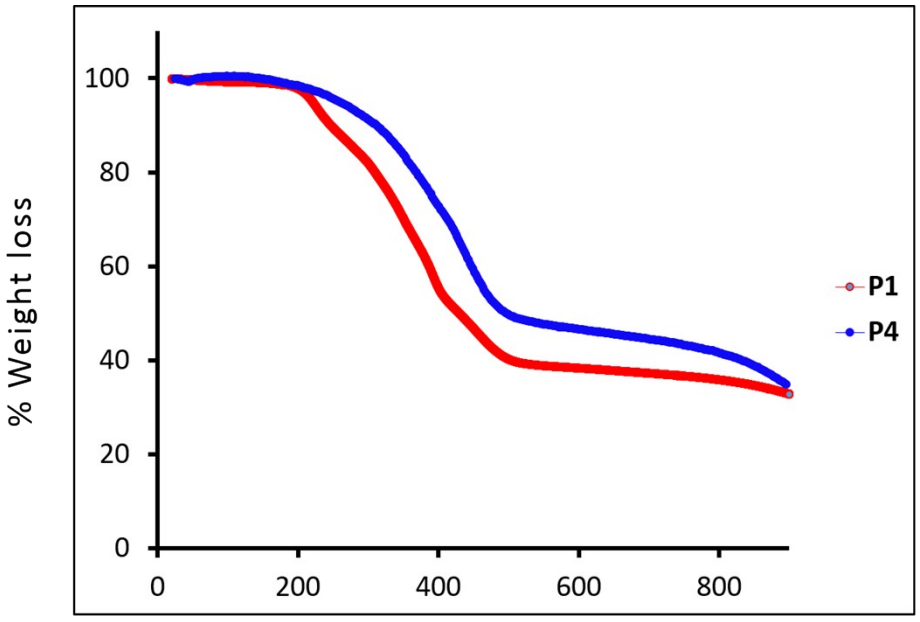

	P1	P4
T_d (°C)[a]	221	261

Figure S18: Thermogravimetric analysis (TGA) of **P1** and **P4** measuring at a heating rate of 10°C.min^{-1} under a 80 mL/min N_2(g) flow. a: the decomposition onset was defined by a 5 wt% loss.

7. The absorption spectra of P1 and P4

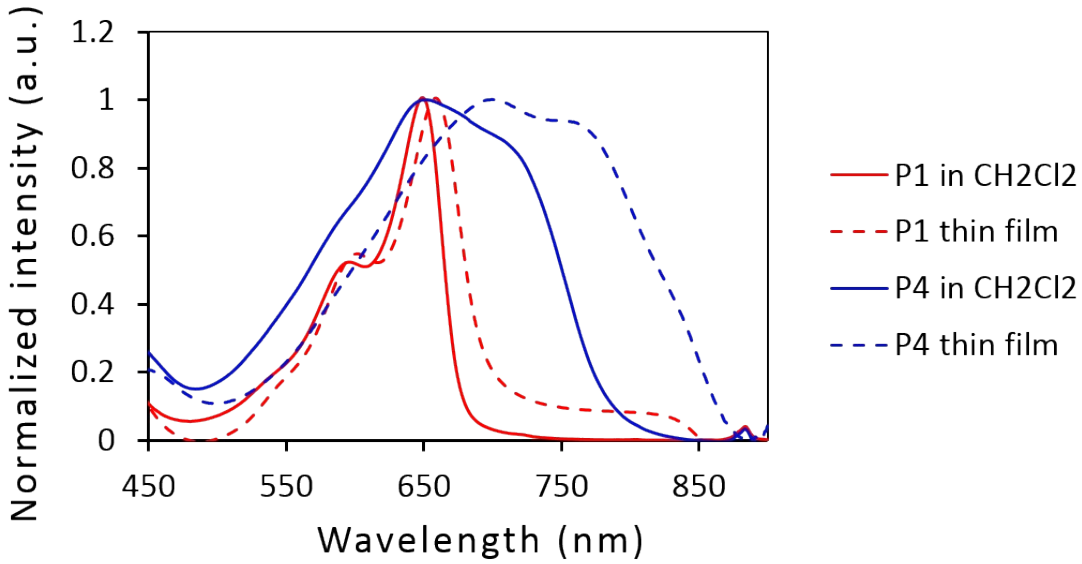

Figure S19: Zoom of the absorption spectra of **P1** and **P4** in CH_2Cl_2 (solid line) as spin coated films on a quartz plate (dashed line). The film thicknesses were 47 and 38 nm, respectively, for **P1** and **P4**.

8. DFT and TD-DFT computations of the ligands Ln

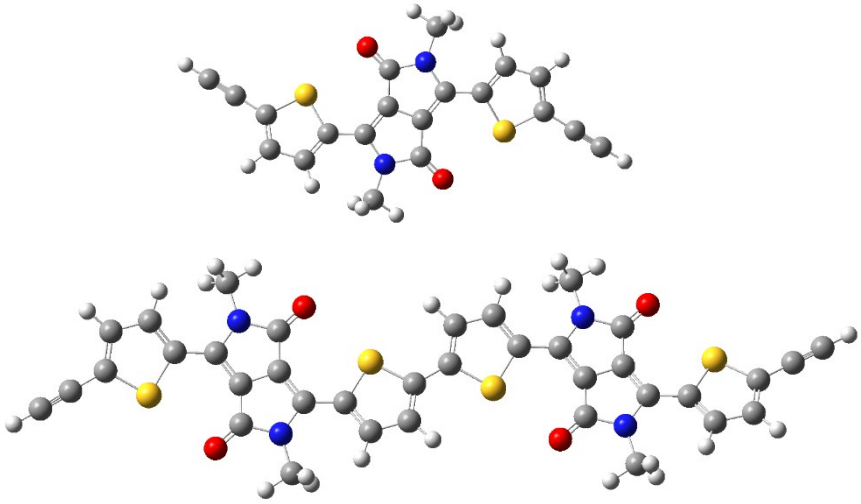

Figure S20: Geometry optimization of **L1** (top) and **L4** (bottom; the $SiMe_3$ groups have been replaced by H to save computation time); C, grey; H, white; S, yellow; N, blue, O, red).

DFT and TD-DFT calculations for **L1**

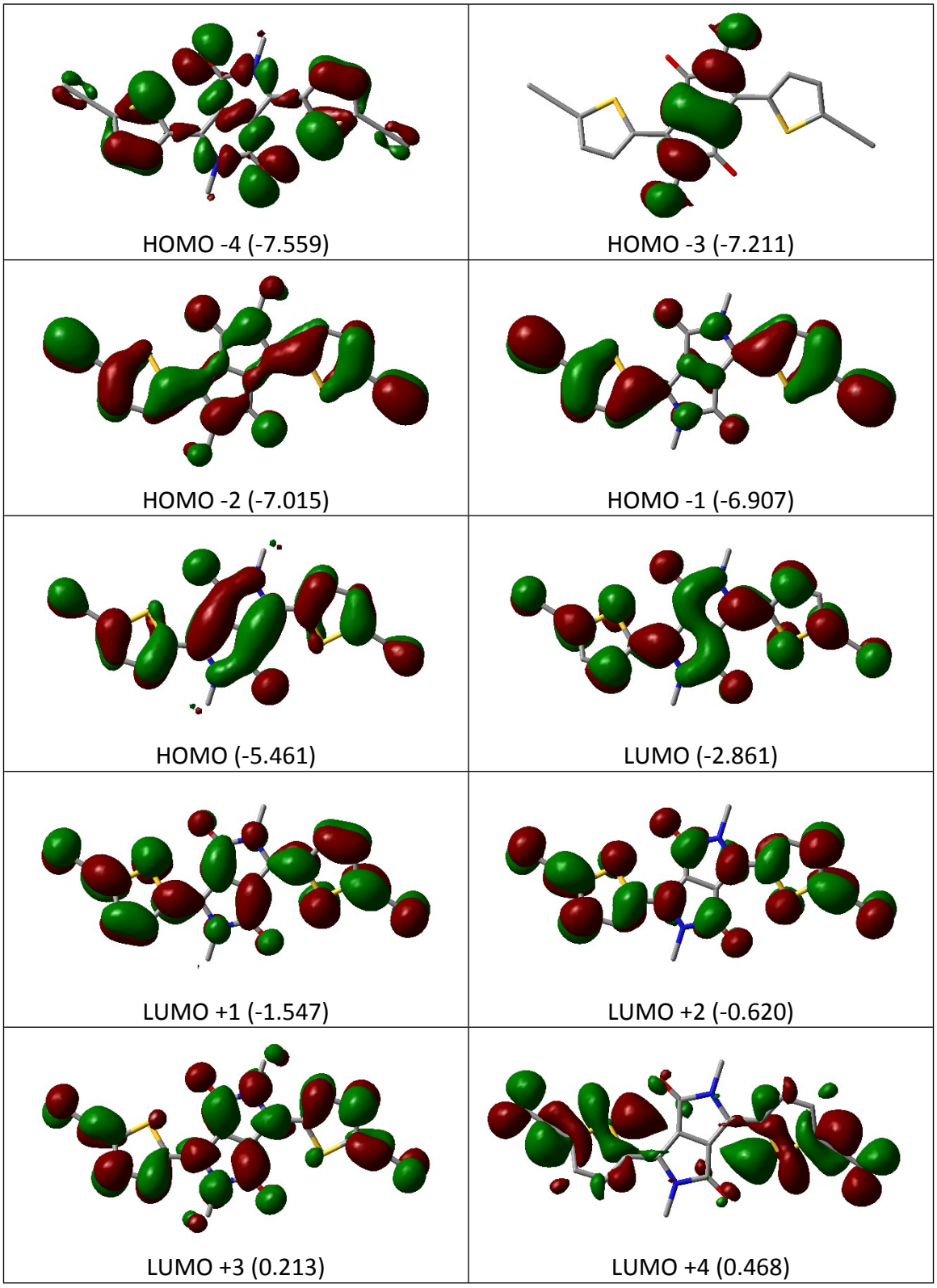

Figure S21: Representations of the frontier MOs for **L1** (energy in eV).

Table S1: Relative atomic contributions (%) of the various fragments to the frontier MOs of **L1**.

Fragments	H-4	H-3	H-2	H-1	HOMO	LUMO	L+1	L+2	L+3	L+4
DPP	29.9	1.8	36.8	**55.1**	27.6	40.5	63.4	**57.5**	36.0	**76.4**
Thiophenes	**68.5**	**98.2**	**42.4**	15.9	**66.2**	**52.5**	**24.2**	27.9	**53.9**	7.2
Ethynyl	1.6	0.1	20.8	29.0	6.2	7.0	12.4	14.6	10.1	16.4

Table S2: Calculated position (λ), oscillator strength (f) and major contributions of the first 100 singlet-singlet electronic transitions for **L1**.

λ (nm)	f	Major contributions
535.4	0.6759	HOMO→LUMO (101%)
383.9	0	H-3→LUMO (14%), H-1→LUMO (18%), HOMO→L+1 (67%)
368.6	0	H-3→LUMO (82%)
356.1	0	H-4→LUMO (87%)
346.5	0.4289	H-2→LUMO (90%)
331.3	0.0001	H-1→LUMO (73%), HOMO→L+1 (23%)
324.4	0.0038	H-7→LUMO (49%), H-5→LUMO (43%)
299.3	0.0583	H-7→LUMO (37%), H-5→LUMO (36%), HOMO→L+2 (20%)
297.7	0.0015	H-6→LUMO (91%)
286.9	0.3424	H-5→LUMO (18%), HOMO→L+2 (65%)
273.3	0.0002	H-8→LUMO (87%)
272.9	0.0001	H-9→LUMO (87%)
257.4	0	H-2→L+1 (52%), HOMO→L+3 (43%)
256.6	0.1626	H-1→L+1 (95%)
249.9	0.0005	H-2→L+1 (26%), HOMO→L+3 (30%), HOMO→L+4 (32%)
249.5	0.0007	H-2→L+1 (17%), HOMO→L+3 (14%), HOMO→L+4 (58%)
248.5	0.0747	H-3→L+1 (91%)
247.1	0.0021	H-4→L+1 (55%), HOMO→L+5 (32%)
246.4	0.0067	H-4→L+1 (32%), HOMO→L+5 (55%)
233.7	0.0434	H-10→LUMO (87%)
233.4	0	H-7→L+1 (21%), H-5→L+1 (49%), HOMO→L+6 (17%)
232.7	0	HOMO→L+6 (68%)
232.0	0.0014	HOMO→L+7 (84%)
226.6	0	H-11→LUMO (55%), H-7→L+1 (32%)
225.3	0.0529	H-6→L+1 (78%)
224.4	0.0016	H-11→LUMO (23%), H-7→L+1 (24%), H-5→L+1 (17%), H-1→L+2 (23%)
217.0	0.0002	H-3→L+2 (88%)
215.8	0.0033	H-5→L+1 (13%), H-1→L+2 (58%)
215.5	0.0157	H-2→L+2 (72%), HOMO→L+8 (17%)
215.0	0	H-9→LUMO (11%), H-8→L+1 (51%), H-4→L+2 (19%)
214.1	0.0043	H-9→L+1 (64%), H-8→LUMO (11%), H-8→L+2 (11%)
210.0	0.0001	H-8→L+1 (18%), H-4→L+2 (61%)
208.6	0.1459	HOMO→L+8 (63%)

206.1	0.0016	H-12→LUMO (10%), HOMO→L+9 (67%)
203.5	0.0167	H-7→L+2 (17%), H-5→L+2 (16%), H-2→L+5 (12%), H-1→L+4 (17%)
203.0	0.0003	H-2→L+4 (33%), H-1→L+5 (37%)
202.3	0.0304	H-7→L+2 (12%), H-2→L+5 (21%), H-1→L+4 (28%)
200.7	0.0013	H-13→LUMO (76%)
198.3	0.0639	H-15→LUMO (32%), H-14→LUMO (25%), H-5→L+2 (26%)
195.7	0.0459	H-15→LUMO (11%), H-7→L+2 (23%), H-5→L+2 (11%), H-1→L+3 (28%)
194.3	0.0008	H-6→L+2 (44%), H-2→L+3 (25%)
193.4	0.0006	H-13→LUMO (10%), H-12→LUMO (46%), H-6→L+2 (23%)
192.3	0.0047	H-2→L+7 (27%), H-1→L+6 (36%)
192.2	0	H-2→L+6 (29%), H-1→L+7 (35%)
189.8	0	H-10→L+1 (82%)
189.6	0.0885	H-15→LUMO (14), H-14→LUMO (13), H-5→L+2 (10%), H-1→L+3 (38%)
189.1	0.0856	H-15→LUMO (17%), H-14→LUMO (31%), H-1→L+3 (12%)
188.3	0.0011	H-6→L+5 (14%), H-5→L+4 (22%), H-2→L+3 (17%)
187.7	0.0025	H-6→L+4 (19%), H-5→L+5 (22%), H-1→L+6 (10%)
186.7	0.0015	H-6→L+2 (10%), H-2→L+3 (39%)
186.1	0.0016	H-11→L+1 (74%)
184.6	0	H-16→LUMO (86%)
184.1	0.0007	H-7→L+2 (25%), H-4→L+3 (61%)
183.4	0.1803	H-3→L+3 (83%)
181.6	0.0001	H-9→L+2 (61%), H-8→L+1 (15%), H-8→L+3 (10%)
181.6	0.0012	H-9→L+1 (17%), H-8→L+2 (63%)
178.8	0.0143	H-3→L+4 (70%), H-3→L+6 (10%)
178.2	0	H-7→L+3 (31%), H-5→L+3 (38%)
177.8	0	H-3→L+5 (14%), H-2→L+4 (37%), H-1→L+5 (33%)
177.1	0.0459	H-3→L+4 (13%), H-2→L+5 (42%), H-1→L+4 (30%)
176.3	0.0004	H-3→L+5 (66%), H-3→L+7 (13%)
174.5	0.1236	H-4→L+4 (46%)
173.6	0	H-7→L+3 (15%), H-4→L+5 (30%)
173.1	0	H-6→L+5 (15%), H-5→L+3 (11%), H-5→L+6 (10%), H-4→L+5 (14%), H-4→L+7 (20%)
172.9	0.0065	H-6→L+3 (19%), H-6→L+4 (11%), H-6→L+6 (13%), H-5→L+7 (22%), H-4→L+6 (11%)
172.1	0	H-6→L+7 (16%), H-5→L+6 (17%), H-1→L+8 (11%)
172.0	0.0008	HOMO→L+10 (86%)
171.7	0.0514	H-6→L+3 (38%)
169.8	0.0002	HOMO→L+11 (90%)
169.7	0.048	H-10→L+2 (12%), H-6→L+3 (26%), H-2→L+8 (18%)
169.6	0.0009	H-7→L+3 (13%), H-5→L+3 (19%), H-1→L+8 (35%)
169.3	0.0005	H-3→L+6 (27%), H-2→L+7 (34%), H-1→L+6 (28%)
169.1	0.0001	H-3→L+7 (14%), H-2→L+6 (37%), H-1→L+7 (33%)
168.4	0.0003	H-19→LUMO (11%), H-17→LUMO (72%)
167.8	0.0031	H-18→LUMO (64%), HOMO→L+12 (12%)
167.8	0.0002	H-3→L+6 (53%), H-2→L+7 (18%), H-1→L+6 (13%)
167.4	0	H-3→L+7 (51%), H-2→L+6 (12%), HOMO→L+12 (10%)
166.9	0.106	H-12→L+1 (11%), H-10→L+2 (36%), H-2→L+8 (22%), H-1→L+9 (15%)

166.7	0	H-18→LUMO (10%), H-3→L+7 (14%), HOMO→L+12 (63%)
166.0	0.0009	H-11→L+2 (14%), H-3→L+8 (60%)
164.8	0.0022	H-11→L+2 (30%), H-3→L+8 (29%), H-1→L+8 (17%)
164.7	0.0018	H-19→LUMO (54%), H-17→LUMO (15%), H-13→L+1 (13%)
164.2	0.0001	H-19→LUMO (12%), H-13→L+1 (27%), H-12→L+1 (31%)
163.7	0.0149	H-4→L+4 (15%), H-4→L+6 (27%), HOMO→L+13 (13%)
163.5	0	H-7→L+4 (15%), H-5→L+4 (20%), H-4→L+5 (33%), H-4→L+7 (10%)
162.9	0.0192	H-12→L+1 (12%), H-5→L+5 (10%), HOMO→L+13 (26%)
162.8	0.0079	H-13→L+1 (14%), H-12→L+1 (21%), H-1→L+9 (12%)
162.5	0.0015	H-15→L+1 (31%), H-14→L+1 (36%)
162.1	0.0004	H-7→L+4 (16%), H-4→L+7 (42%)
161.8	0.1279	H-7→L+5 (15%), H-5→L+5 (17%), H-4→L+6 (21%), HOMO→L+13 (12%)
161.5	0	H-8→L+3 (10%), H-4→L+8 (53%)
161.3	0.0092	H-21→LUMO (49%), H-16→L+1 (10%)
160.4	0.0001	H-2→L+9 (32%), H-1→L+8 (12%)
160.2	0.0272	H-9→L+3 (39%), H-8→L+2 (11%)
159.8	0.0576	H-3→L+9 (20%), H-1→L+9 (19%), HOMO→L+13 (19%)
159.7	0.0001	H-8→L+3 (32%), H-4→L+8 (13%)
159.6	0.0351	H-9→L+4 (12%), H-8→L+5 (10%)
159.0	0.0002	H-8→L+3 (15%), H-6→L+5 (13%), H-2→L+9 (13%)
158.9	0.1234	H-3→L+9 (14%)
158.7	0.0001	H-15→L+1 (13%), H-7→L+4 (10%), H-6→L+5 (17%)

DFT and TD-DFT calculations for **L4**

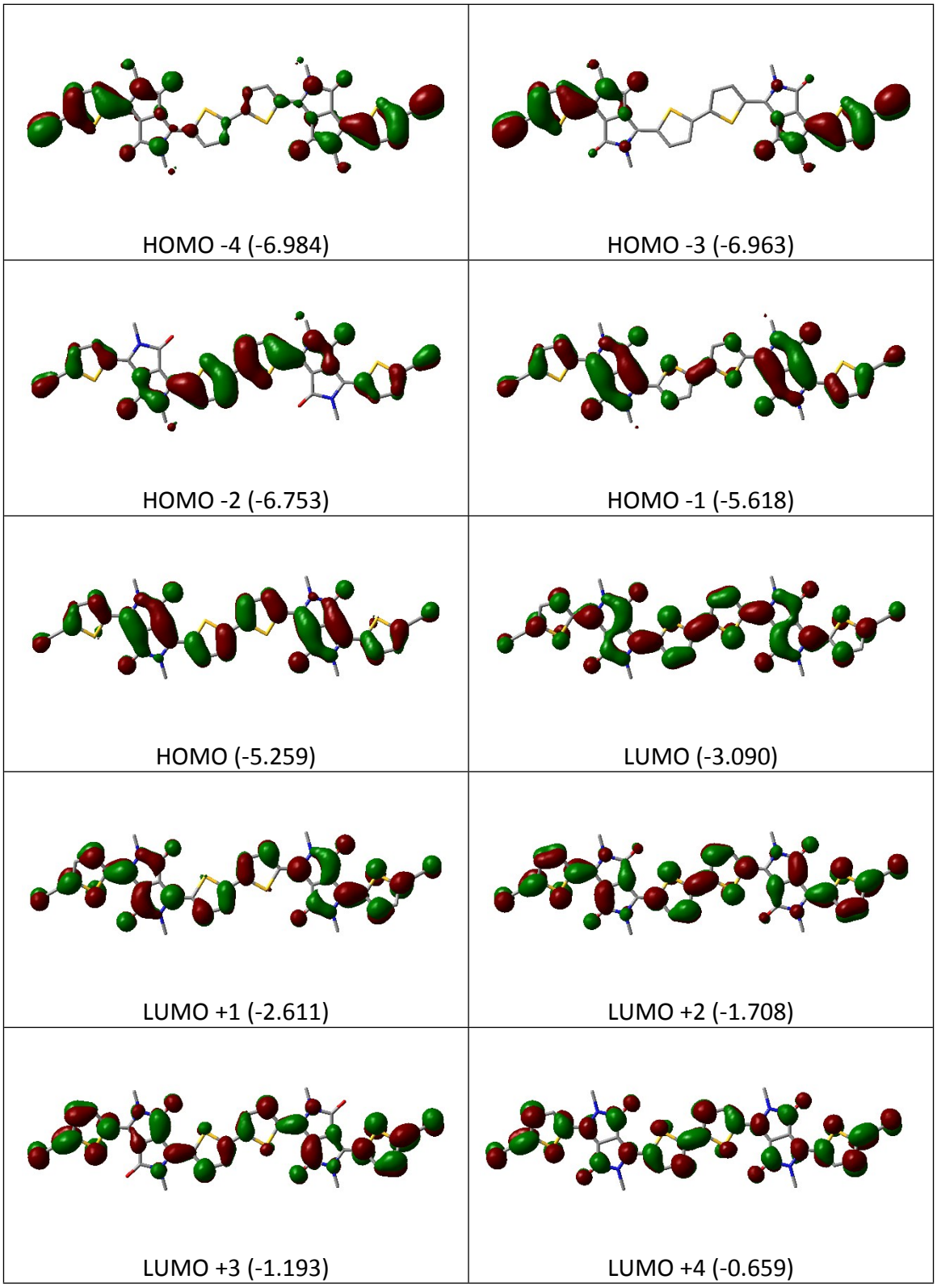

Figure S22: Representations of the frontier MOs for **L4** (energy in eV).

Table S3: Relative atomic contributions (%) of the various fragments to the frontier MOs of **L4**.

Fragments	H-4	H-3	H-2	H-1	HOMO	LUMO	L+1	L+2	L+3	L+4
DPP	39.6	**44.2**	**64.2**	25.0	36.8	47.2	41.6	**68.2**	**58.9**	**61.1**
Thiophenes	**41.3**	31.7	30.5	**71.7**	**60.3**	**49.9**	**53.9**	25.7	32.5	30.9
Ethynyl	19.2	24.1	5.2	3.3	2.9	2.8	4.5	6.1	8.6	8.0

Table S4: Calculated position, oscillator strength (f) and major contributions of the first 100 singlet-singlet electronic transitions for **L4**.

λ (nm)	f	Major contributions
669.2	1.7075	HOMO→LUMO (100%)
579.5	0	H-1→LUMO (78%), HOMO→L+1 (20%)
513.2	0	H-1→LUMO (21%), HOMO→L+1 (79%)
466.3	0.177	H-1→L+1 (97%)
410.7	0.0322	H-2→LUMO (25%), HOMO→L+2 (69%)
379.7	0.3429	H-6→LUMO (13%), H-4→LUMO (17%), H-2→LUMO (49%), HOMO→L+2 (11%)
378.3	0	H-6→L+1 (17%), H-5→LUMO (57%), H-1→L+2 (14%)
374.4	0.0877	H-6→LUMO (61%), H-5→L+1 (17%)
369.7	0	H-5→LUMO (17%), H-3→LUMO (27%), H-1→L+2 (27%), HOMO→L+3 (13%)
360.1	0	H-8→L+1 (18%), H-7→LUMO (61%)
359.6	0.0376	H-8→LUMO (53%), H-7→L+1 (18%), H-4→LUMO (12%)
355.5	0.0003	H-3→LUMO (33%), H-1→L+2 (38%), HOMO→L+3 (10%)
353.6	0.1514	H-8→LUMO (13%), H-4→LUMO (50%), H-2→LUMO (15%)
337.8	0.0006	H-3→LUMO (24%), HOMO→L+3 (56%)
329.0	0	H-2→L+1 (71%)
327.5	0.0001	H-14→L+1 (10%), H-13→LUMO (38%), H-9→LUMO (21%)
327.4	0.0078	H-14→LUMO (31%), H-13→L+1 (14%), H-10→LUMO (28%)
316.3	0.0456	H-4→LUMO (11%), H-3→L+1 (25%), H-1→L+3 (46%)
313.7	0.0004	H-11→LUMO (30%), H-9→LUMO (46%)
310.6	0.0007	H-4→L+1 (81%)
309.1	0.2324	H-3→L+1 (56%), H-1→L+3 (35%)
304.7	0.0159	H-14→LUMO (17%), H-10→LUMO (35%), HOMO→L+4 (14%)
304.4	0.0011	H-13→LUMO (20%), H-11→LUMO (41%), H-9→LUMO (14%)
302.8	0.02	H-14→LUMO (10%), H-12→LUMO (61%)
301.8	0.006	H-6→LUMO (18%), H-5→L+1 (60%)
301.0	0	H-6→L+1 (70%), H-5→LUMO (21%)
294.3	0.4291	H-10→LUMO (10%), HOMO→L+4 (52%)
287.2	0.0081	H-8→LUMO (21%), H-7→L+1 (67%)
286.2	0	H-8→L+1 (64%), H-7→LUMO (21%)

280.1	0.0441	H-11→L+1 (11%), H-9→L+1 (74%)
279.8	0.002	H-15→LUMO (13%), H-1→L+4 (54%), HOMO→L+5 (16%)
276.1	0.0001	H-17→LUMO (64%), H-16→L+1 (23%)
276.0	0.0001	H-17→L+1 (23%), H-16→LUMO (65%)
273.5	0	H-15→LUMO (26%), H-12→L+1 (25%), H-10→L+1 (25%)
271.0	0.0693	H-2→L+2 (91%)
270.1	0	H-10→L+1 (23%), H-1→L+4 (27%), HOMO→L+5 (28%)
268.4	0.0082	H-11→L+1 (61%), H-10→LUMO (10%)
266.7	0	H-15→LUMO (24%), H-12→L+1 (49%)
264.6	0.0011	H-15→LUMO (22%), H-14→L+1 (13%), H-10→L+1 (16%), HOMO→L+5 (28%)
262.1	0.0023	H-14→LUMO (11%), H-13→L+1 (38%), HOMO→L+6 (20%)
260.6	0.0008	H-14→L+1 (53%), H-13→LUMO (17%), H-10→L+1 (10%)
260.3	0.0035	H-13→L+1 (21%), H-4→L+2 (16%), HOMO→L+6 (20%)
257.2	0.0015	H-3→L+2 (86%)
256.4	0.0775	H-4→L+2 (50%), HOMO→L+7 (20%)
253.0	0.0188	H-4→L+2 (13%), H-1→L+5 (23%), HOMO→L+7 (36%)
250.7	0.0001	H-1→L+7 (19%), HOMO→L+8 (56%), HOMO→L+10 (10%)
249.8	0.0085	H-6→L+2 (13%), H-1→L+8 (22%), HOMO→L+7 (13%), HOMO→L+9 (38%)
249.5	0.0605	H-6→L+2 (60%), HOMO→L+9 (13%)
248.9	0.001	H-5→L+2 (72%)
247.7	0.0001	H-1→L+9 (18%), HOMO→L+10 (54%)
245.9	0.0004	H-2→L+3 (79%)
244.6	0.0196	H-15→L+1 (17%), H-8→L+2 (21%), H-1→L+5 (18%), HOMO→L+6 (19%)
244.4	0	H-8→L+3 (12%), H-7→L+2 (66%)
243.5	0.0218	H-8→L+2 (48%), H-7→L+3 (10%)
241.1	0.109	H-15→L+1 (56%), H-1→L+5 (25%)
239.2	0	H-17→LUMO (30%), H-16→L+1 (56%)
239.2	0.002	H-17→L+1 (57%), H-16→LUMO (31%)
239.0	0	H-19→LUMO (16%), H-1→L+6 (45%), HOMO→L+11 (15%)
234.8	0.0262	H-18→LUMO (68%)
234.4	0	H-19→LUMO (34%), H-9→L+2 (26%)
233.9	0.0001	H-9→L+2 (12%), H-1→L+12 (17%), HOMO→L+12 (12%), HOMO→L+13 (37%)
233.9	0.0014	H-1→L+13 (19%), HOMO→L+12 (43%), HOMO→L+13 (14%)
232.7	0	H-9→L+2 (24%), H-4→L+3 (40%)
232.3	0.0017	H-10→L+2 (25%), H-3→L+3 (39%)
230.3	0.0008	H-19→LUMO (13%), H-11→L+2 (28%), H-9→L+2 (15%), H-4→L+3 (15%)
229.4	0.0002	H-13→L+2 (16%), H-11→L+2 (20%), H-1→L+7 (14%)
229.1	0.0072	H-14→L+2 (17%), H-10→L+2 (16%), H-3→L+3 (31%)
227.3	0	H-13→L+2 (18%), H-6→L+3 (13%), H-1→L+7 (19%)
227.0	0.0028	H-6→L+4 (13%), H-5→L+3 (57%)
226.8	0	H-6→L+3 (48%), H-5→L+4 (12%), H-1→L+7 (13%)
225.2	0.0546	H-14→L+2 (12%), H-12→L+2 (33%), H-5→L+3 (11%), H-2→L+4 (18%)
224.7	0.0411	H-14→L+2 (20%), H-12→L+2 (19%), H-10→L+2 (20%)

224.5	0.0009	H-1→L+6 (18%), HOMO→L+11 (37%)
224.0	0.0035	H-13→L+2 (24%), H-11→L+2 (25%), HOMO→L+11 (11%)
223.7	0.0017	H-1→L+10 (72%)
220.5	0.0174	H-7→L+3 (24%), H-2→L+4 (36%)
220.1	0.0003	H-8→L+3 (48%), H-7→L+2 (10%), H-7→L+4 (14%)
219.4	0.0024	H-14→L+2 (21%), H-7→L+3 (30%), H-2→L+4 (19%)
217.2	0	H-1→L+7 (18%), H-1→L+9 (42%), HOMO→L+8 (32%)
217.2	0.0013	H-1→L+8 (54%), HOMO→L+7 (10%), HOMO→L+9 (23%)
214.3	0.1788	H-1→L+11 (66%)
213.5	0.0001	H-18→L+1 (28%), H-3→L+4 (19%)
213.3	0.0118	H-19→L+1 (13%), H-9→L+3 (26%), H-4→L+4 (15%)
213.2	0.0001	H-21→LUMO (10%), H-18→L+1 (11%), H-17→L+2 (11%), HOMO→L+15 (11%)
212.9	0.0012	H-20→LUMO (16%), H-9→L+3 (11%), H-4→L+4 (15%), HOMO→L+14 (24%)
212.2	0.0061	H-17→L+1 (11%), H-17→L+3 (13%), H-16→L+2 (32%), H-9→L+3 (15%)
212.2	0.0006	H-18→L+1 (10%), H-17→L+2 (12%), H-3→L+4 (39%)
211.6	0.0005	H-19→L+1 (36%), H-4→L+4 (31%)
211.5	0.0012	H-21→LUMO (48%), H-17→L+2 (15%)
210.7	0.0403	H-19→L+1 (19%), H-11→L+3 (15%), H-9→L+3 (20%), HOMO→L+14 (12%)
210.7	0.0007	H-21→LUMO (15%), H-18→L+1 (25%), H-10→L+3 (10%), HOMO→L+15 (14%)
208.4	0.005	H-20→LUMO (33%), H-11→L+3 (12%)
208.3	0.0001	H-15→L+2 (51%), H-5→L+4 (16%)
207.5	0.0004	H-12→L+3 (13%), H-10→L+3 (10%), H-5→L+4 (18%)
207.2	0.0489	H-6→L+4 (47%), H-5→L+3 (14%)
207.1	0	H-15→L+2 (19%), H-5→L+4 (31%)
206.3	0.0771	H-20→LUMO (18%), H-6→L+4 (13%), HOMO→L+14 (12%)
205.6	0	H-1→L+12 (35%), HOMO→L+13 (23%)
205.6	0.0144	H-1→L+13 (35%), HOMO→L+12 (22%)
204.7	0.0003	H-14→L+3 (17%), H-12→L+3 (46%)

TD-DFT simulated absorption spectra for **L1-L4**.

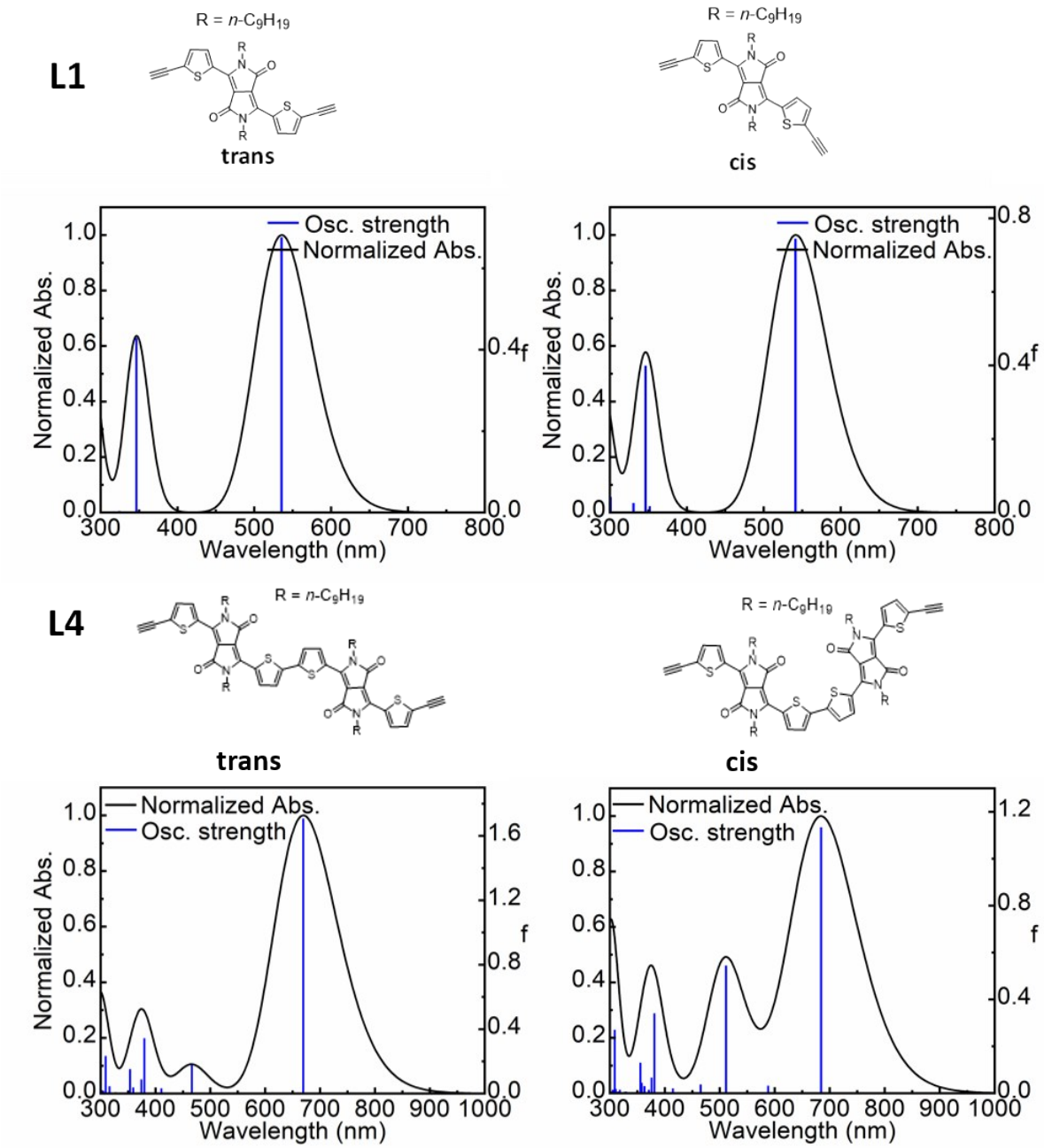

Figure S23: Bar graph reporting the calculated oscillator strength and calculated position of the electronic transitions calculated by TDDFT for **L1** (top) and **L4** (bottom; bar graph; f = computed oscillator strength. The simulated absorptions are generated using a Full width at half maximum (FWHM) of 3000 $cm^{-1.}$

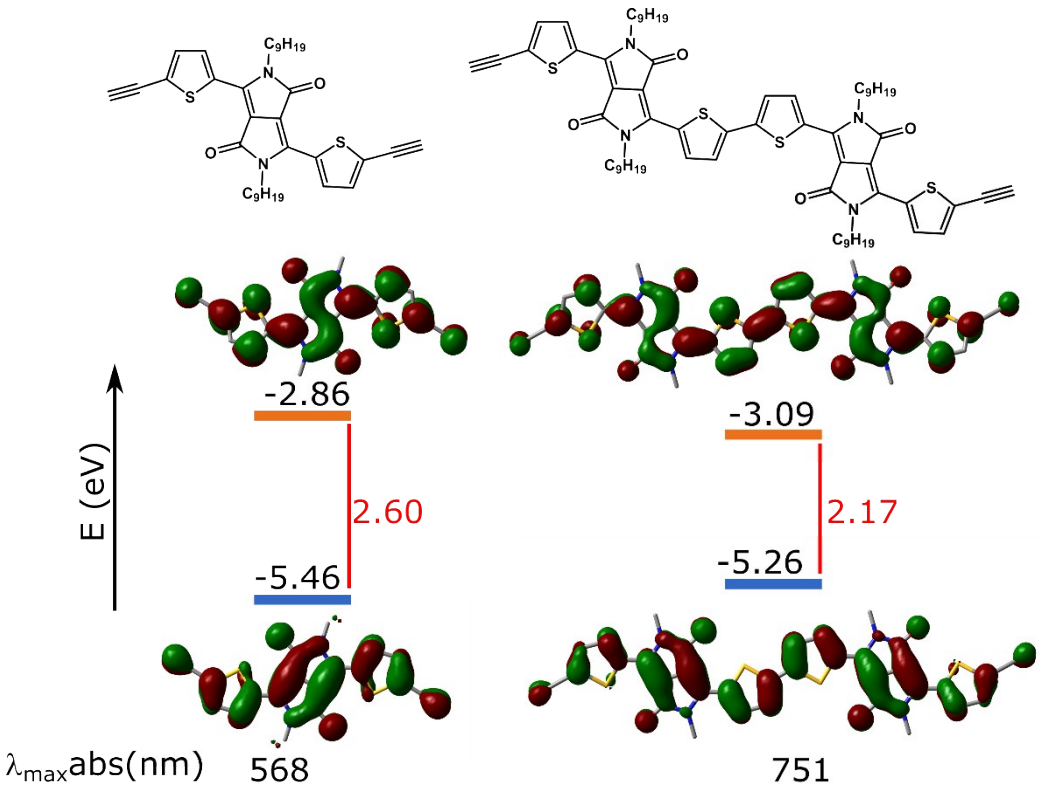

Figure S24: Comparison of the calculated HOMO and LUMO energies (in eV) of the ligands using models **L1** and **L4**

9. DFT and TD-DFT computations of the metallooligomers Pn

DFT and TD-DFT calculation for model **P1.**

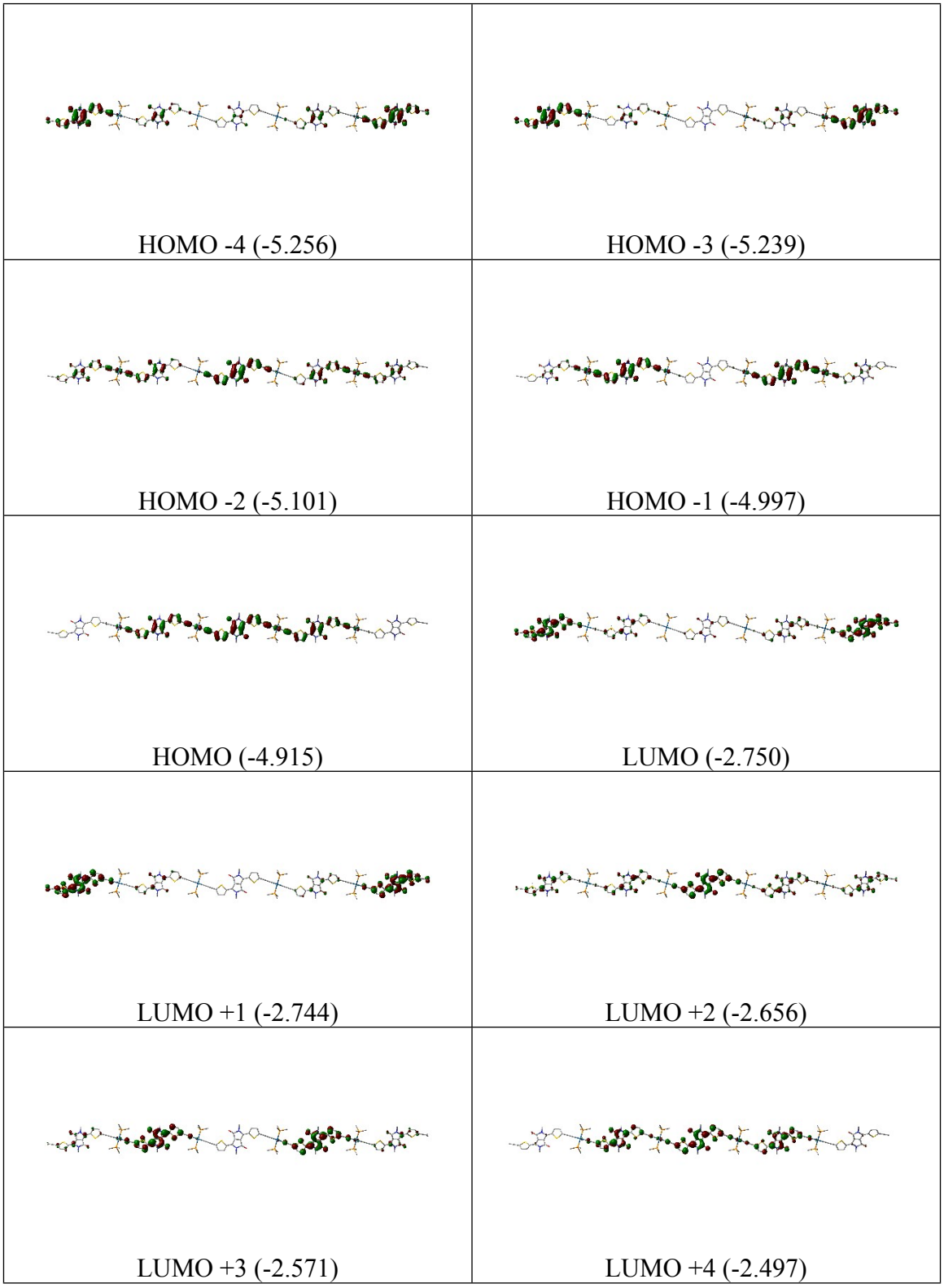

Figure S25: Representations of the frontier MOs for **P1** (energy in eV).

Table S5: Relative atomic contributions (%) of the various fragments to the frontier MOs of **P1**.

Fragments	H-4	H-3	H-2	H-1	HOMO	LUMO	L+1	L+2	L+3	L+4
Thiophène	23.4	22.6	28.7	30.4	32.1	32.3	32.5	37.9	38.0	38.2
Platine	1.6	3.2	5.2	7.4	8.7	2.2	2.0	3.1	3.0	2.8
DPP	**66.8**	**64.3**	**54.4**	**48.2**	**44.1**	**58.7**	**58.8**	**52.5**	**52.8**	**53.2**
Ethynyl	8.1	9.9	11.8	14.0	15.1	6.8	6.8	6.6	6.2	5.7

Table S6: Calculated position (λ), oscillator strength (f) and major contributions of the first 100 singlet-singlet electronic transitions for **P1**.

λ(nm)	f	Major contributions
675.0	5.8501	H-1→L+1 (14%), HOMO→LUMO (30%), HOMO→L+2 (39%)
650.2	0.0158	H-1→LUMO (33%), HOMO→L+1 (44%)
622.4	0.092	H-1→L+1 (19%), HOMO→LUMO (24%), HOMO→L+2 (45%)
605.7	0.0086	H-1→LUMO (20%), H-1→L+2 (12%), HOMO→L+1 (52%)
602.8	0.5161	H-2→LUMO (15%), H-1→L+1 (33%), HOMO→LUMO (44%)
591.2	0.0068	H-1→LUMO (22%), H-1→L+2 (23%), HOMO→L+3 (46%)
573.8	0.4507	H-3→L+1 (11%), H-2→LUMO (29%), H-2→L+2 (12%), H-1→L+1 (29%)
570.9	0.0001	H-1→L+2 (45%), HOMO→L+3 (34%)
569.4	0.005	H-3→LUMO (10%), H-2→L+1 (53%), H-1→LUMO (19%)
564.5	0.2178	H-2→LUMO (24%), H-1→L+3 (11%), HOMO→L+4 (47%)
555.2	0.0102	H-4→L+1 (35%), H-3→LUMO (36%), H-2→L+1 (22%)
554.8	0.0128	H-2→LUMO (18%), H-2→L+2 (45%), H-1→L+3 (13%), HOMO→L+4 (18%)
551.0	0.3072	H-4→LUMO (28%), H-3→L+1 (29%), HOMO→L+4 (22%)
544.9	0.1545	H-2→L+2 (26%), H-2→L+4 (13%), H-1→L+3 (36%), HOMO→L+2 (13%)
535.8	0.0007	H-2→L+3 (40%), H-1→L+4 (50%)
520.8	0	H-2→L+3 (48%), H-1→L+4 (40%)
511.2	0.0757	H-2→L+4 (80%), H-1→L+3 (13%)
509.6	0.0062	H-4→LUMO (48%), H-3→L+1 (46%)
509.5	0.0007	H-4→L+1 (48%), H-3→LUMO (46%)
504.7	0.0107	H-4→L+3 (29%), H-3→L+2 (60%)
503.8	0.1229	H-4→L+2 (56%), H-3→L+3 (31%)
480.3	0.0125	H-4→L+2 (38%), H-4→L+4 (11%), H-3→L+3 (49%)
479.8	0.0021	H-4→L+3 (51%), H-3→L+2 (34%), H-3→L+4 (13%)
460.9	0.0003	H-4→L+3 (18%), H-3→L+4 (80%)
460.1	0.0057	H-4→L+4 (82%), H-3→L+3 (17%)
446.5	0.0049	H-6→L+1 (14%), H-5→LUMO (35%), H-5→L+2 (29%)
443.3	0.0381	H-7→L+1 (12%), H-6→LUMO (27%), H-5→L+1 (38%)
436.4	0.015	H-7→LUMO (15%), H-6→L+1 (16%), H-5→L+2 (36%)
427.5	0.4206	H-7→L+1 (11%), H-6→L+2 (23%), H-5→L+3 (31%)
421.1	0.0004	H-7→LUMO (10%), H-5→LUMO (42%), HOMO→L+5 (14%)
420.7	0.0727	H-7→L+1 (12%), H-5→L+1 (54%)

418.9	0.0067	H-6→L+3 (12%), H-5→L+4 (35%)
414.5	0.0014	H-5→LUMO (10%), H-5→L+2 (16%), HOMO→L+5 (34%), HOMO→L+7 (13%)
413.1	0.1687	H-8→L+2 (14%), H-6→LUMO (10%), H-6→L+2 (15%), H-6→L+4 (11%), H-1→L+5 (18%)
405.2	0.0492	H-6→L+2 (13%), H-5→L+3 (38%), HOMO→L+6 (14%)
404.0	0.0019	H-8→L+1 (10%), H-7→LUMO (13%), H-7→L+2 (10%), H-6→L+1 (43%)
402.9	0.2602	H-7→L+3 (15%), H-6→LUMO (22%), H-6→L+2 (14%)
400.4	0.009	H-7→L+2 (11%), H-3→L+6 (12%), H-2→L+5 (10%)
399.9	0.2201	H-8→L+2 (12%), H-7→L+1 (10%), H-7→L+3 (11%), H-6→LUMO (24%)
394.6	0.0054	H-5→L+4 (31%), H-1→L+6 (10%), HOMO→L+7 (15%)
387.2	0.0459	H-7→L+1 (23%), H-1→L+7 (11%)
386.4	0.0061	H-1→L+5 (12%), HOMO→L+6 (56%)
386.0	0	H-8→L+3 (10%), H-6→L+3 (36%), H-5→L+2 (10%), H-5→L+4 (12%)
385.1	0.0006	H-7→LUMO (10%)
384.4	0.0178	H-16→LUMO (19%), H-15→L+1 (19%)
383.7	0	H-8→L+1 (29%), H-7→LUMO (20%)
383.0	0.031	H-8→LUMO (56%), H-7→L+1 (19%)
381.8	0	H-8→L+1 (21%), H-4→L+5 (12%), H-3→L+6 (13%)
381.2	0	HOMO→L+5 (32%), HOMO→L+7 (37%)
379.8	0.0006	H-8→L+4 (12%), H-6→L+4 (42%)
378.0	0.0002	H-13→L+3 (12%), H-12→L+2 (20%), H-11→L+2 (35%)
376.6	0.0001	H-14→L+2 (11%), H-13→L+2 (41%), H-11→L+3 (13%)
375.7	0.0005	H-7→L+2 (15%), H-2→L+7 (10%), H-1→L+6 (33%)
374.1	0.1397	H-4→L+6 (10%), H-1→L+7 (26%), HOMO→L+8 (24%)
373.5	0.0018	H-8→L+2 (36%), H-8→L+4 (11%), H-7→L+3 (20%), H-6→L+2 (10%), H-6→L+4 (12%)
372.0	0.0001	H-8→L+3 (19%), H-7→L+2 (21%), H-7→L+4 (16%), H-2→L+5 (18%), H-1→L+6 (14%)
368.3	0.0639	H-2→L+6 (48%), H-1→L+5 (22%)
366.3	0.0002	H-2→L+5 (17%)
365.7	0	H-19→L+2 (10%), H-11→L+4 (13%)
365.5	0.0008	H-29→LUMO (16%), H-29→L+1 (12%), H-28→LUMO (11%), H-28→L+1 (16%)
365.1	0.0004	H-1→L+7 (35%), HOMO→L+8 (31%)
364.6	0.0001	H-29→LUMO (13%), H-29→L+1 (10%), H-28→LUMO (10%), H-28→L+1 (14%)
364.2	0.0003	
363.1	0.0002	H-21→L+2 (28%), H-21→L+4 (22%)
362.3	0.0004	H-23→L+2 (14%), H-23→L+4 (11%), H-22→L+3 (26%)
362.0	0.0001	H-23→L+3 (22%), H-22→L+2 (13%)
360.7	0	H-21→L+2 (13%), H-12→L+4 (11%)
359.9	0.0223	H-8→L+4 (36%), H-7→L+3 (26%)
359.7	0.0001	H-8→L+3 (28%), H-7→L+4 (55%)
358.9	0.015	H-20→L+2 (10%), H-14→L+4 (12%), H-13→L+4 (23%), H-12→L+3 (10%)
358.5	0.0038	H-2→L+7 (25%)
357.8	0.2606	H-10→LUMO (14%), H-9→L+1 (11%)

355.9	0	H-2→L+7 (22%), H-1→L+8 (11%)
353.0	0.001	H-9→L+2 (20%), H-1→L+8 (23%), HOMO→L+9 (12%)
352.9	0.0536	H-8→L+4 (10%), H-2→L+8 (23%), H-1→L+9 (14%)
350.7	0.0038	H-9→LUMO (10%), HOMO→L+9 (33%)
350.5	0.0219	
349.4	0.0003	H-40→LUMO (12%), H-39→LUMO (10%), H-39→L+1 (14%)
348.9	0.0177	H-40→LUMO (16%), H-40→L+1 (12%), H-39→LUMO (10%), H-39→L+1 (14%)
347.4	0.0031	H-4→L+5 (20%), H-4→L+7 (16%), H-3→L+8 (11%)
346.5	0.0049	H-4→L+8 (10%), H-3→L+5 (17%), H-3→L+7 (15%)
343.9	0.1092	H-10→L+2 (23%), H-9→L+1 (32%)
342.6	0	H-32→L+2 (16%), H-9→LUMO (13%)
342.3	0.0012	H-4→L+5 (14%), H-3→L+6 (16%)
341.7	0.0123	H-4→L+6 (39%), H-3→L+5 (23%)
341.5	0.0028	H-34→L+3 (18%), H-33→L+2 (12%)
341.5	0.0007	H-9→L+2 (13%), H-4→L+5 (13%), H-3→L+6 (27%)
340.6	0.0246	H-2→L+8 (33%), H-1→L+9 (33%)
340.3	0	H-34→L+2 (11%), H-32→L+2 (11%), H-32→L+4 (18%)
338.2	0.0001	H-10→L+1 (17%), H-10→L+3 (12%), H-9→LUMO (20%), H-9→L+4 (13%), H-2→L+9 (13%)
337.1	0.2396	H-9→L+1 (24%), H-9→L+3 (18%)
337.1	0.0047	H-10→L+1 (15%), H-2→L+9 (10%)
335.6	0.0656	H-10→LUMO (12%), H-9→L+3 (20%)
334.9	0.1692	H-10→LUMO (42%)
334.4	0.0005	H-10→L+1 (27%), H-2→L+9 (11%)
334.2	0.0008	H-4→L+7 (43%)
334.1	0.0631	H-11→L+1 (10%), H-3→L+7 (33%)
333.7	0.0079	H-14→LUMO (10%), H-13→LUMO (12%), H-12→L+1 (21%), H-11→L+1 (18%)
333.7	0.0009	H-13→L+1 (14%), H-12→LUMO (17%), H-11→LUMO (26%)
333.3	0.3551	H-1→L+9 (11%), HOMO→L+10 (55%)

DFT and TD-DFT calculations for model **P4**

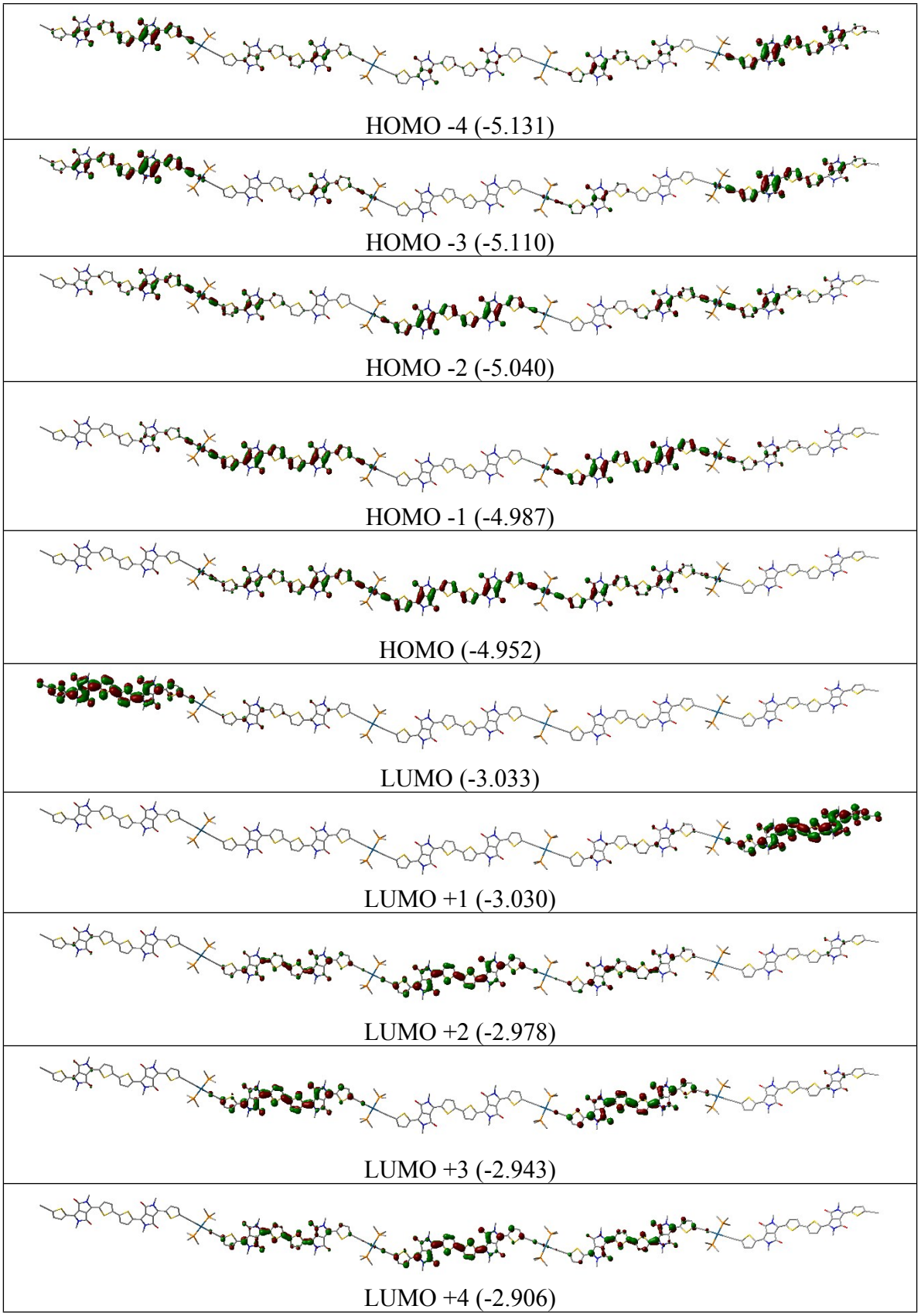

Figure S26: Representations of the frontier MOs for model **P4** (energy in eV).

Table S7: Relative atomic contributions (%) of the various fragments to the frontier MOs of model **P4**.

Fragments	H-4	H-3	H-2	H-1	HOMO	LUMO	L+1	L+2	L+3	L+4
Thiophène	36.3	35.3	36.5	37.1	37.5	41.1	47.2	47.0	47.3	47.6
DPP	**58.7**	**54.8**	**52.0**	**49.6**	**48.3**	**55.4**	**49.3**	**48.9**	**48.7**	**48.5**
platine	1.0	3.2	4.0	4.8	5.3	0.6	0.6	1.3	1.3	1.3
Ethynyl	4.1	6.7	7.5	8.5	8.9	2.9	2.9	2.8	2.7	2.6

Table S8: Calculated positions (λ), oscillator strengths (f) and major contributions of the first 30 singlet-singlet electronic transitions for model **P4**.

λ(nm)	f	Major contributions
779.1	11.1885	H-2→L+4 (10%), H-1→L+3 (18%), HOMO→L+2 (44%)
757.2	0.0998	H-1→LUMO (10%), H-1→L+2 (14%), HOMO→L+3 (15%)
731.6	0.3912	H-3→L+1 (11%), HOMO→L+2 (17%)
707.1	0.002	H-1→L+2 (22%), HOMO→L+3 (23%)
690.6	0.0175	H-2→L+2 (21%), H-1→L+3 (28%), HOMO→L+4 (30%)
687.5	0.2072	H-3→L+1 (20%), HOMO→L+1 (62%)
686.6	0.3747	H-4→LUMO (17%), HOMO→LUMO (64%)
670.7	0.0774	H-4→LUMO (14%), H-1→LUMO (57%), HOMO→LUMO (17%)
670.1	0.1007	H-3→L+1 (12%), H-1→L+1 (61%), HOMO→L+1 (16%)
656.0	0.0005	H-1→L+2 (35%), H-1→L+4 (10%), HOMO→L+3 (33%)
652.0	0.0211	H-2→LUMO (53%), HOMO→L+4 (10%)
650.5	0.0018	H-2→L+1 (61%)
646.4	0.0231	H-2→LUMO (11%), H-2→L+2 (30%), HOMO→L+4 (34%)
641.1	0.0034	H-2→L+3 (33%), H-1→L+4 (35%), HOMO→L+3 (11%)
638.6	0.1924	H-2→L+2 (20%), H-2→L+4 (23%), H-1→L+3 (20%), HOMO→L+2 (32%)
621.9	0.0021	H-3→L+2 (13%), H-2→L+3 (14%), H-1→L+4 (24%), HOMO→L+3 (13%)
618.8	0.0007	H-4→L+2 (15%), H-3→L+3 (27%), H-2→L+4 (20%)
615.5	0.0061	H-4→L+3 (14%), H-3→L+2 (16%), H-2→L+3 (23%), H-1→L+2 (14%)
611.9	0.0018	H-4→LUMO (25%), H-3→LUMO (64%)
611.1	0.1022	H-3→L+3 (10%), H-2→L+4 (31%), H-1→L+3 (18%)
609.9	0.0167	H-4→L+1 (62%), H-3→L+1 (28%)
602.6	0.0002	H-5→L+2 (27%), H-4→L+3 (15%), H-3→L+4 (10%)
599.6	0.0934	H-5→L+1 (15%)
598.0	0.0053	H-5→LUMO (12%), H-5→L+4 (10%)
589.3	0.1495	H-8→L+1 (15%), H-5→L+3 (10%), H-4→L+2 (27%)
587.9	0.0235	H-9→LUMO (20%), H-6→L+3 (12%), H-3→L+2 (13%)
584.4	0.0327	H-8→L+1 (20%), H-5→L+1 (44%)
583.7	0.0422	H-9→LUMO (18%), H-5→LUMO (45%)
583.5	0.0732	H-6→L+2 (10%), H-4→L+2 (11%), H-3→L+3 (24%)
581.6	0.0147	H-4→L+3 (34%), H-3→L+2 (20%)

572.0	0.0032	H-4→L+4 (10%), H-3→L+3 (14%), H-3→L+4 (53%)
569.5	0.005	H-4→L+3 (10%), H-4→L+4 (57%), H-3→L+3 (11%), H-3→L+4 (10%)
566.3	0.0023	H-7→LUMO (10%), H-6→LUMO (48%), H-5→LUMO (22%)
566.1	0.0019	H-6→L+1 (49%), H-5→L+1 (21%)
563.9	0.0001	H-5→L+2 (18%), HOMO→L+5 (15%), HOMO→L+7 (22%)
558.4	0.0052	H-5→L+3 (26%), H-1→L+5 (18%), HOMO→L+6 (20%)
551.8	0.0027	H-7→L+3 (11%), H-6→L+2 (27%), H-5→L+3 (27%)
549.9	0.0031	H-7→LUMO (17%), H-1→L+6 (10%)
548.1	0.0021	H-7→LUMO (36%), H-5→L+4 (12%), HOMO→L+7 (11%)
547.5	0.0011	H-7→L+1 (53%), H-5→L+4 (10%)
545.6	0.0004	H-7→LUMO (15%), H-7→L+1 (17%), H-7→L+2 (12%), H-5→L+4 (30%)
542.1	0.0089	H-6→L+2 (17%), H-6→L+4 (18%), H-1→L+7 (16%), HOMO→L+6 (18%)
539.5	0.0034	H-7→L+2 (19%), H-7→L+4 (12%), H-2→L+5 (10%), HOMO→L+5 (19%)
538.3	0.0202	HOMO→L+6 (27%)
537.4	0.0014	HOMO→L+5 (26%), HOMO→L+7 (14%)
532.8	0.0107	H-7→L+3 (10%), H-6→L+4 (19%), H-1→L+7 (27%), HOMO→L+8 (22%)
529.0	0.0065	H-4→L+5 (11%), H-2→L+7 (11%), H-1→L+5 (10%), H-1→L+6 (28%)
527.9	0.0909	H-4→L+6 (12%), H-3→L+5 (16%), H-3→L+6 (11%), H-1→L+5 (16%)
523.5	0.0001	H-7→L+3 (35%), H-6→L+2 (10%), H-6→L+4 (26%)
523.0	0.0005	H-3→L+6 (11%), H-2→L+7 (15%), H-1→L+8 (20%), HOMO→L+9 (20%)
521.6	0.0019	H-4→L+5 (11%), H-2→L+5 (22%), H-1→L+7 (10%), HOMO→L+8 (13%)
521.2	0.0003	H-2→L+5 (13%), H-1→L+7 (11%), HOMO→L+8 (16%)
520.2	0.0004	H-7→L+4 (44%), H-6→L+3 (18%)
519.1	0.0045	H-4→L+6 (11%), H-2→L+6 (43%)
513.8	0.0004	H-2→L+5 (14%), H-2→L+7 (43%), HOMO→L+9 (25%)
510.1	0.0142	H-2→L+9 (20%), H-1→L+8 (25%), HOMO→L+7 (15%), HOMO→L+9 (15%)
509.8	0.0777	H-2→L+8 (32%), H-1→L+9 (26%)
508.8	0	H-8→LUMO (98%)
508.3	0	H-9→L+1 (98%)
502.4	0.0012	H-9→L+2 (50%), H-9→L+3 (35%)
502.0	0.0019	H-8→L+2 (45%), H-8→L+3 (39%)
499.4	0.1585	H-4→L+8 (13%), H-3→L+7 (30%), H-1→L+9 (17%)
497.6	0.0007	H-4→L+7 (31%), H-3→L+8 (26%), H-2→L+9 (11%)
495.7	0.0211	H-2→L+8 (38%), H-1→L+7 (10%), H-1→L+9 (25%)
494.6	0.0027	H-4→L+5 (27%), H-3→L+5 (38%), H-3→L+6 (18%)
492.8	0.0009	H-4→L+6 (52%), H-3→L+5 (14%), H-3→L+6 (10%)
491.3	0.0003	H-2→L+9 (45%), H-1→L+8 (17%)
488.6	0.0316	H-8→L+2 (46%), H-8→L+3 (24%), H-8→L+4 (11%)
488.2	0.0888	H-9→L+2 (28%), H-9→L+3 (16%), H-5→L+5 (11%)
487.8	0.1416	H-9→L+2 (18%), H-9→L+3 (22%), H-5→L+5 (13%)
486.0	0.003	H-6→L+5 (20%), H-5→L+6 (30%)

483.1	0.0025	H-6→L+6 (11%), H-5→L+7 (18%), H-3→L+9 (10%)
479.4	0.0009	H-8→L+3 (24%), H-8→L+4 (71%)
478.5	0.0012	H-9→L+3 (18%), H-9→L+4 (66%)
478.2	0.0003	H-9→L+4 (10%), H-4→L+7 (29%), H-3→L+8 (28%)
475.2	0.0176	H-5→L+7 (16%), H-4→L+8 (23%), H-3→L+7 (26%)
472.4	0.0005	H-6→L+7 (27%), H-5→L+6 (17%), H-5→L+8 (16%)
471.8	0.0189	H-7→L+7 (15%), H-6→L+8 (20%), H-5→L+5 (14%), H-5→L+9 (13%), H-4→L+8 (13%)
469.5	0.0276	H-9→L+5 (29%), H-5→L+6 (14%)
468.9	0.1912	H-8→L+6 (34%), H-5→L+5 (14%)
465.8	0.0165	H-4→L+8 (10%), H-3→L+9 (49%)
464.3	0.0041	H-4→L+9 (48%)
463.1	0.0093	H-6→L+5 (27%), H-5→L+8 (12%), H-4→L+9 (14%)
462.0	0.0134	H-7→L+7 (10%), H-6→L+6 (34%), H-3→L+9 (11%)
457.8	0.0934	H-13→L+1 (11%), H-12→L+1 (30%), H-11→L+1 (22%), H-10→L+1 (11%)
457.5	0.0959	H-13→LUMO (21%), H-12→LUMO (23%), H-11→LUMO (20%), H-10→LUMO (11%)
454.6	0.0007	H-6→L+5 (10%), H-6→L+7 (31%), H-5→L+8 (31%)
453.8	0.0035	H-7→L+5 (48%), H-5→L+9 (16%)
452.9	0.086	H-10→L+2 (57%)
452.7	0.0006	H-7→L+6 (61%)
449.2	0.0021	H-13→L+2 (12%), H-11→L+2 (32%), H-10→L+3 (25%)
448.2	0.0366	H-7→L+5 (10%), H-7→L+9 (14%), H-6→L+8 (23%), H-5→L+7 (14%), H-5→L+9 (27%)
447.3	0.0195	H-7→L+7 (38%), H-7→L+9 (12%), H-6→L+8 (10%)
444.2	0.0008	H-7→L+8 (28%), H-6→L+9 (38%)
439.4	0.0021	H-12→L+2 (10%), H-11→L+3 (22%), H-10→L+4 (36%)
437.9	0.0014	H-13→L+2 (23%), H-12→L+3 (21%), H-11→L+4 (22%)
436.5	0.0029	H-13→L+3 (19%), H-12→L+2 (10%), H-12→L+4 (10%), H-10→LUMO (22%)
435.8	0.0025	H-13→L+4 (12%), H-11→L+2 (13%), H-10→LUMO (12%), H-10→L+1 (26%)
433.0	0.0012	H-7→L+8 (37%), H-6→L+9 (31%)
431.9	0.0045	H-13→L+3 (13%), H-10→LUMO (31%), H-10→L+1 (20%)

TD-DFT simulated absorption spectra of the models **P1-P4**

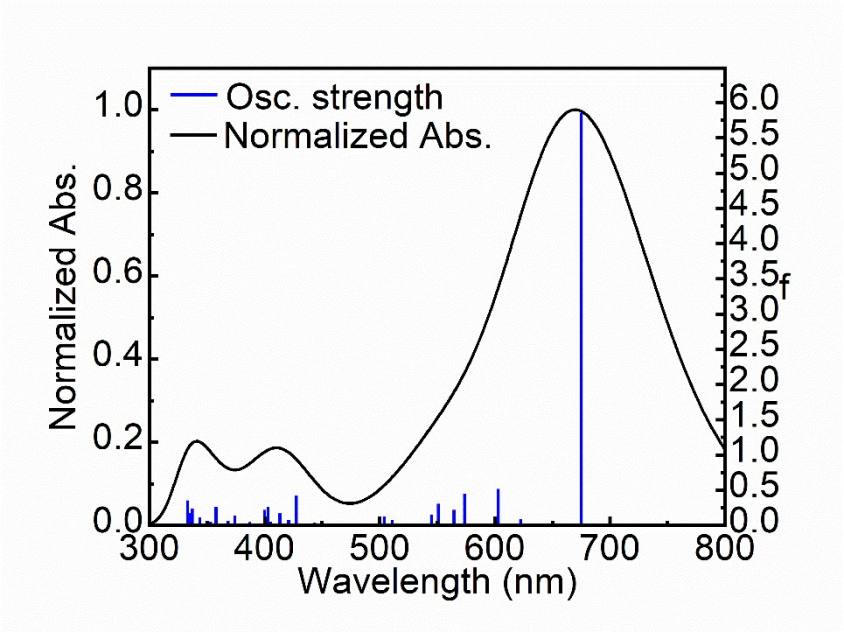

Figure S27: Bar graph reporting the calculated oscillator strength and calculated position of the electronic transitions calculated by TDDFT for model **P1** (bar graph; f = computed oscillator strength). The simulated absorptions are generated using a Full width at half maximum (FWHM) of 1000 cm^{-1}.

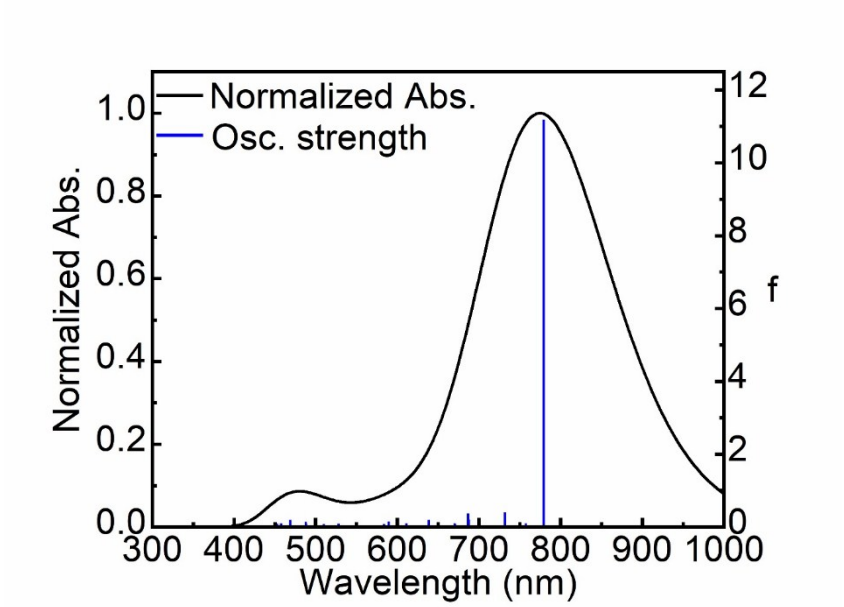

Figure S28: Bar graph reporting the calculated oscillator strength and calculated position of the electronic transitions calculated by TDDFT for model **P4** (bar graph; f = computed oscillator strength). The simulated absorptions are generated using a Full width at half maximum (FWHM) of 3000 cm^{-1}.

10. Emission spectroscopy

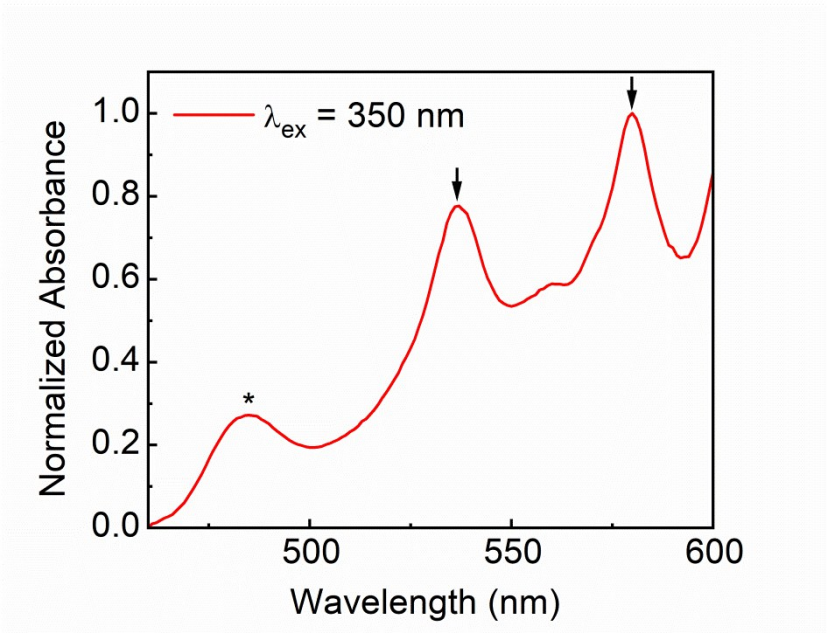

Figure S29: Emission spectrum of **P1** in 2MeTHF at 77 K. The signal labelled with a star (*) is an artifact associated with the Dewar+solvent assembly. The signals at 537 and 560 nm are an emission arising from the triplet state of the **[Pt]**-moiety.

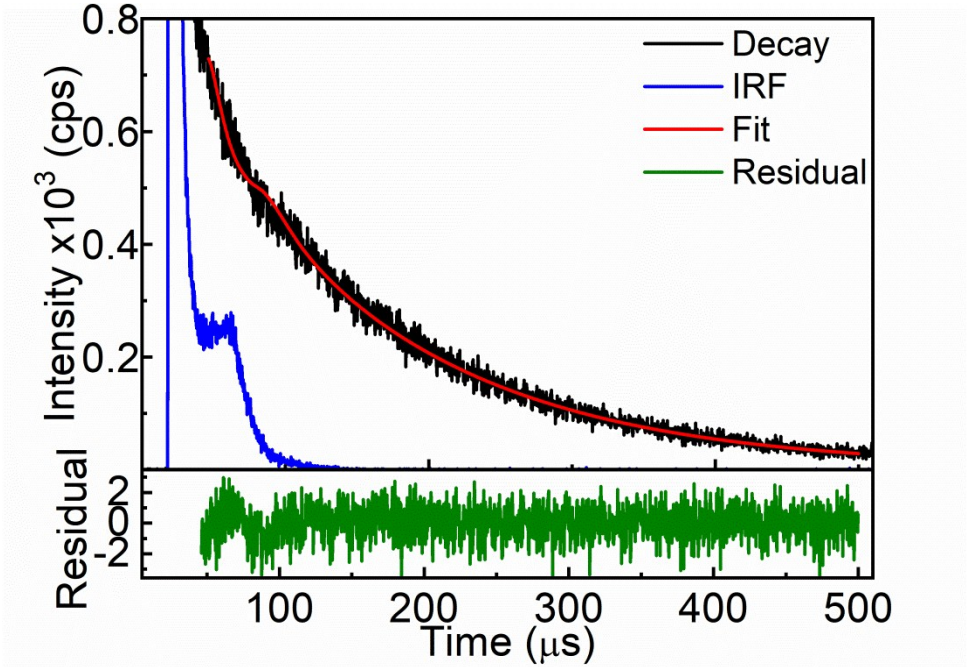

Figure S30: Emission decay (black) of the signal at λ_{em} = 537 nm for **P1** in 2MeTHF at 77K, residuals (green), IRF (blue) and best fit (red). Multi-exponential analysis yields τ_P = 13.2 μs (11.4), 150 μs (88.6 %), χ^2 = 1.096. λ_{exc}= 350 nm.

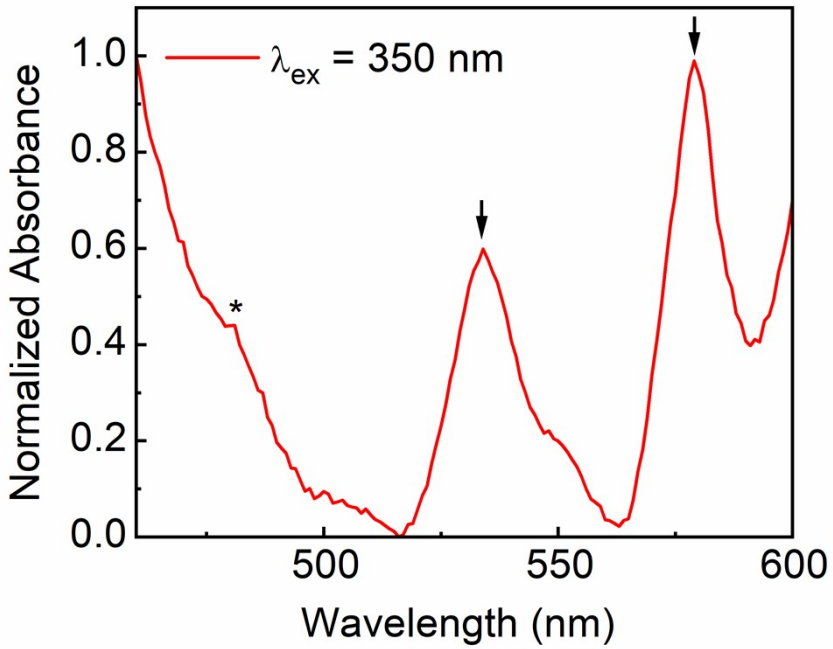

Figure S31: Emission spectrum of **P4** in 2MeTHF at 77 K. The signal labelled with a star (*) is an artifact associated with the Dewar+solvent assembly. The signals at 537 and 560 nm are an emission arising from the triplet state of the **[Pt]**-moiety.

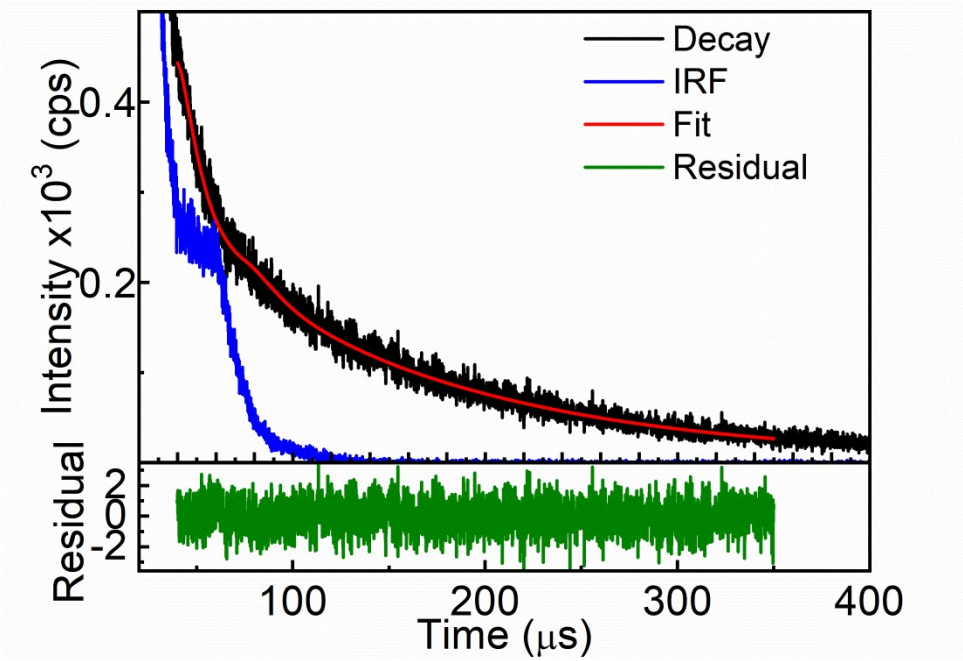

Figure S32: Emission decay (black) of the signal at λ_{em} = 537 nm for **P4** in 2MeTHF at 77K, residuals (green), IRF (blue) and best fit (red). Multi-exponential analysis yields τ_P = 11.1 μs (18.9), 130 μs (81.1%), χ^2 = 1.000. λ_{exc}= 350 nm.